



# Chimera: Improving Generalist Model with Domain-Specific Experts

Tianshuo Peng<sup>1,2,\*</sup>, Mingsheng Li<sup>3,\*</sup>, Jiakang Yuan<sup>3</sup>, Hongbin Zhou<sup>1</sup>, Renqiu Xia<sup>1,4</sup>, Renrui Zhang<sup>2</sup>  
 Lei Bai<sup>1</sup>, Song Mao<sup>1</sup>, Bin Wang<sup>1</sup>, Aojun Zhou<sup>2</sup>, Botian Shi<sup>1</sup>  
 Tao Chen<sup>3,5</sup>, Bo Zhang<sup>1,†,✉</sup>, Xiangyu Yue<sup>2,✉</sup>

<sup>1</sup>Shanghai Artificial Intelligence Laboratory, <sup>2</sup>MMLab, The Chinese University of Hong Kong

<sup>3</sup>College of Future Information Technology, Fudan University, <sup>4</sup>Shanghai Jiao Tong University

<sup>5</sup>Shanghai Innovation Institute

\* Equal Contribution, ✉ Corresponding Authors, † Project Lead

## Abstract

Large Multi-modal Models (LMMs), trained on web-scale datasets predominantly composed of natural images, have demonstrated remarkable performance on general tasks. However, these models often exhibit limited specialized capabilities for domain-specific tasks that require extensive domain prior knowledge. An intuitive solution is to post-train LMMs on a specific domain, but often suffers from the labor-intensive annotating process and the inaccessibility of private training data. Directly integrating expert models tailored for those tasks is also challenging due to representational gaps and imbalanced optimization. To address these challenges, we introduce **Chimera**, a scalable and low-cost multi-modal pipeline designed to boost the ability of existing LMMs with domain-specific experts. Specifically, we design a progressive training strategy to integrate features from expert models into the input of a generalist LMM. To address the imbalanced optimization caused by the well-aligned general visual encoder, we introduce a novel Generalist-Specialist Collaboration Masking (GSCM) mechanism. This results in a versatile model that excels across the chart, table, math, and document domains, achieving state-of-the-art performance on multi-modal reasoning and visual content extraction tasks, both of which are challenging tasks for assessing existing LMMs. We will release model weights, along with the data used for training and evaluation, to facilitate future research on LMMs.

## 1. Introduction

The past year has witnessed the remarkable success of Large Multi-modal Models (LMMs) in handling a variety of general domain tasks, such as image captioning [10, 14, 41], visual dialog [4, 11, 12, 59, 78], and cross-modal re-

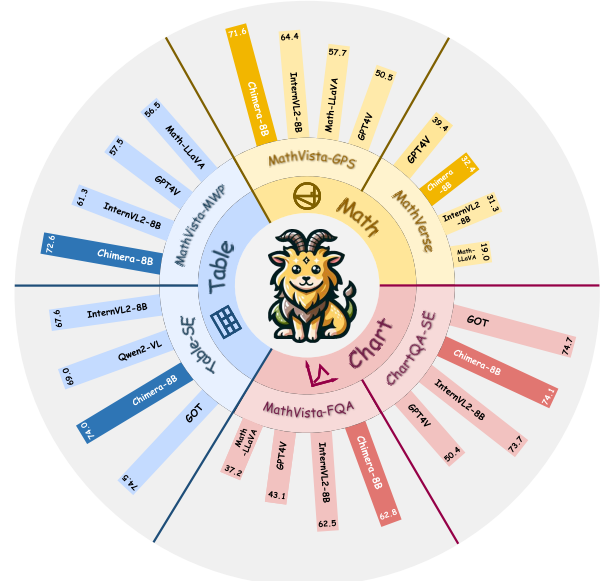


Figure 1. Performance comparison of different models on multi-modal reasoning (MathVista, MathVerse) and visual structural extraction (ChartQA-SE, Table-SE) tasks.

trieval [7, 84], demonstrating their potential as a technical pathway towards a general-purpose AI assistant. Although proficient in a wide range of tasks, their performance still lags behind that of models fine-tuned with target-domain data, especially in **specialized tasks** such as *multi-modal reasoning* and *visual content extraction*. As depicted in Fig. 1, state-of-the-art general-purpose LMMs demonstrate significant limitations in addressing these tasks, highlighting the necessity for further research to bridge this gap.

Current research on LMMs [10, 12, 40, 59, 60, 62, 85] has extensively invested in scaling up by collecting web-scale image-text pairs and employing multi-task instruction tuning to develop generalist models, following a “One for

All” paradigms [12, 77]. However, the pursuit of generality often results in suboptimal performance in domain-specific tasks, such as Chart [84], Table [83], and Math [20, 89, 93]. This is mainly due to the substantial differences between natural images and those found in specialized fields [37]. For instance, domain-specific tasks such as multi-modal reasoning and visual structural extraction often involve content that includes charts, tables, geometric figures, and function graphs [17, 83, 84, 92]. These tasks are characterized by higher text density and more abstract content [75, 80]. As a result, general LMMs, which are primarily trained on web-scale natural images, struggle to adapt effectively to these specialized contexts [30, 84, 89].

To enhance performance in target domains, numerous studies have focused on developing tailored models or task-specific architectures for downstream tasks [17, 67, 80, 83, 84, 89, 92], adopting a “One for One” paradigm where models are trained on a single scene type. While these expert models exhibit strong capabilities in specialized tasks, they are often criticized for being designed to address individual scenarios. This phenomenon arises from significant distribution gaps across various sub-domains, such as tables, charts, functions, and geometry, potentially sacrificing their generalizability across broader applications using specialized models.

To push the boundary further for the existing LMMs and improve their performance in specialized domains, an intuitive solution is to **post-train** LMMs on data relevant to the target domain. However, a common challenge is that the vast amounts of domain-specific data necessary for specialist models are often proprietary and inaccessible. On the other hand, integrating specialist experts that contain specialized prior knowledge presents a promising approach to address this issue [66, 94]. Moreover, directly combining specialist experts with the generalist model could result in unsatisfactory performance, due to the following factors: 1) large distribution shifts between cross-domain encoders, 2) imbalanced optimization for generalists and specialists.

To address these challenges, this work introduces **Chimera**: a flexible and scalable pipeline that can effectively scale up off-the-shelf experts into LMMs at low cost. Specifically, we utilize a lightweight routing module that dynamically selects tokens from the most suitable experts based on visual content, enabling tailored input to the LLM. Through cost-effective training aimed at feature alignment, we integrate multiple encoders from different expert models into a single LMM, effectively merging diverse specialized knowledge without requiring vast amounts of target-domain data. Besides, we observed alignment imbalances during the cross-modal encoder fusion and propose a General-Expert Collaboration Masking mechanism to facilitate better model fusion. Our method easily adapts LMMs, such as InternVL [12, 13], to a range

of domain-specific tasks, including advanced mathematical reasoning, table/chart QA & extraction, and document structural extraction tasks. By aggregating multiple expert models into a single general LMM, Chimera develops a versatile model endowed with multiple specialized capabilities. During inference, Chimera employs a simple routing module to determine whether to invoke the corresponding domain expert model based on the visual input, resulting in a versatile model that excels across the chart, table, math, and document domains, as well as tasks involving multi-modal reasoning and extraction.

We conduct extensive experiments to evaluate Chimera’s capabilities in multi-modal reasoning and visual content extraction, both of which are challenging domains for assessing existing LMMs. With the introduction of domain knowledge from expert models and supervised fine-tuning, Chimera achieves overall accuracies of 64.9 and 32.4 on the multi-modal reasoning benchmarks MathVista [48] and MathVerse [90], setting a new State-Of-The-Art (SOTA) for LMMs of comparable scale. Direct preference optimization can further boost Chimera’s reasoning capabilities, allowing it to achieve superior performance with a small amount of data. It also surpasses or matches the performance of representative expert models in visual content extraction tasks across chart, table, and document domains.

Our contributions can be summarized as follows:

1. We introduce Chimera, a scalable pipeline that integrates specialist models into generalist LMMs, facilitating their adaptation to many specialized tasks.
2. We present a lightweight routing module that dynamically selects the most relevant experts based on visual input, coupled with Generalist-Specialist Collaboration Masking (GSCM) aimed at facilitating representation alignment between the generalist and domain experts.
3. Chimera achieves SOTA performance on challenging benchmarks for reasoning, including MathVista and MathVerse. Furthermore, it achieves near-specialist-level results in visual structural extraction on benchmarks like ChartQA-SE, Table-SE, Doc-SE, *etc.*

## 2. Related Work

**Generalist Large Multi-modal Models.** Following the remarkable success of Large Language Models (LLMs) [6, 73, 74], researchers have made great efforts in adapting LLMs for multi-modal tasks in a general context, contributing to the flourishing of Large Multi-modal Models (LMMs) [10, 12, 34, 40, 51, 59, 60, 62, 85]. Recent LMMs typically utilize a cross-modal connector [12, 32] and perform the pre-training on large-scale natural image-text datasets [35, 83] to alleviate the modality gap between the visual encoder and the LLMs. For instance, BLIP series [31, 32] utilizes captions from datasets like COCO [39], CC3M [65], SBU [61], and LAION [64], while the LLaVA

series [44, 45] constructs complex instruction-following datasets based on natural images from COCO [39] to further enhance their understanding of visual content.

However, the pursuit of generality often results in limited performance in specialized scenarios, such as geometric and function reasoning [17, 82, 86, 89], table and chart understanding [75, 84, 92], of which the visual content differing significantly from natural images. Moreover, fine-tuning LMMs on specialized domains remains challenging due to inaccessible private data and potential degradation in general performance.

**Expert Models on Specialized Scenarios.** Expert tasks in multimodal settings, such as geometric and function reasoning [82, 89, 90], table and chart understanding [84, 92], and document information extraction [75], often require specialized designs to achieve optimal task performance. For example, Math-LLaVA [67], and MAVIS [89] train LMMs on carefully curated mathematical datasets using natural language descriptions. Table-LLaVA [92] constructs a large-scale multimodal table understanding dataset, while StructEqTable [83] uses extensive table format transformation data to build a highly specialized expert model with limited generality. Similarly, ChartGemma [55] and ChartInstruct [54] train LMMs on diverse chart instruction-following data, and ChartVLM [84] employs a router structure to selectively engage different decoders for base perception tasks and cognition tasks. GOT [80] trains a specialist model on million-scale private data specifically for document structural extraction task. Besides, some work executes complex and challenging tasks, including automated scientific discovery, in the form of multi-agents through carefully designed and comprehensive workflows [71].

While expert models excel in specific domains, they struggle with tasks outside their specialization. In contrast, Chimera integrates specialized knowledge into a generalist LMM, achieving superior performance across both multimodal reasoning and document context extraction tasks.

### 3. Methodology

To develop an assistant that can adapt to challenging domains at a low cost, we propose Chimera, a scalable multimodal model built upon existing LMMs and pretrained expert models. In this section, we first introduce an overview of Chimera in Sec. 3.1. Sec. 3.2 discusses the integration of generalists and domain-specific experts, and Sec. 3.3 details Generalist-Specialist Collaboration Masking (GSCM), an effective method for collaboration between the generalist model and specialists. Furthermore, we present the training recipe for Chimera in Sec. 3.4.

#### 3.1. Overview

As illustrated in Fig 2, Chimera consists of: a general visual encoder  $E^g$ , a general projector  $P^g$  together with a language Model  $f$  initialized from a pretrained LMM, a router

$R$ , an expert model set  $S^e$  with  $N_e$  expert models and corresponding expert projector set  $S^p$ . Assuming expert models from the domains of table, chart, and math as aggregation targets, we have:

$$\begin{aligned} S^e &= \{E^{table}, E^{chart}, E^{math}\} \\ S^p &= \{P^{table}, P^{chart}, P^{math}\}. \end{aligned} \quad (1)$$

**Generalist Branch.** For visual input  $\mathcal{X}_v$ ,  $E^g$  provides the general visual features  $\mathcal{Z}_v = E^g(\mathcal{X}_v)$ ,  $P^g$  projects general visual features into word embedding space, yielding general visual tokens  $\mathcal{H}_v = P^g(\mathcal{Z}_v)$ . During training, we apply the GSCM mechanism on  $\mathcal{H}_v$  as  $\mathcal{H}_v^m$  to replace  $\mathcal{H}_v$ .

**Specialist Branch.** The linear layer  $R$  first predicts routing value  $\mathcal{H}_r \in R^{N_e+1}$  as  $\mathcal{H}_r = R(\mathcal{Z}_v^{cls})$ , where  $\mathcal{Z}_v^{cls}$  represents the classification token of  $\mathcal{Z}_v$ , determining whether to invoke an expert model and which specific expert model to call. Consequently, the expert visual tokens  $\mathcal{H}_e$  can be formulated as:

$$\begin{aligned} i &= \arg \max_i (\mathcal{H}_r)_i \\ \mathcal{H}_e &= \begin{cases} \emptyset, & \text{if } i == 0, \\ S_i^p(S_i^e(\mathcal{X}_v)), & \text{otherwise.} \end{cases} \end{aligned} \quad (2)$$

Given the text embedding  $\mathcal{H}_t$  of instruction  $\mathcal{X}_t$ , the input sequence during training is formulated as:

$$\mathcal{H}_{input} = \text{concat}([\mathcal{H}_v^m : \mathcal{H}_e : \mathcal{H}_t]). \quad (3)$$

We validated Chimera’s capability and adaptability in two distinctly different task scenarios: multi-modal reasoning and visual content extraction, both of which are challenging domains for assessing existing LMMs. The former scenario requires integrating expert models including those for tables, math, and charts. The latter scenario requires integrating expert models that specialize in document structural extraction.

#### 3.2. Integration of Generalist and Specialist

There are two intuitive ideas to adapt an generalist LMM into specialized domain: 1) performing supervised fine-tuning on domain-specific data (naive finetune) and 2) sequentially appending features from different encoders (naive concat). The primary difference between Chimera and these two approaches lies in the definition of the input sequence during training for the language model  $f$ . Let  $\mathcal{H}_{input}^{nf}$  and  $\mathcal{H}_{input}^{nc}$  denote the input sequences in the naive finetune and naive concat methods, respectively. They can be formulated as:

$$\begin{aligned} \mathcal{H}_{input}^{nf} &= \text{concat}([\mathcal{H}_v : \mathcal{H}_t]), \\ \mathcal{H}_{input}^{nc} &= \text{concat}([\mathcal{H}_v : \mathcal{H}_e : \mathcal{H}_t]). \end{aligned} \quad (4)$$

The former approach attempts to use a single visual encoder to handle all visual content, which refuses to incorporate domain-specific knowledge from expert models. Fine-tuning on subtasks in several specialized domains can also

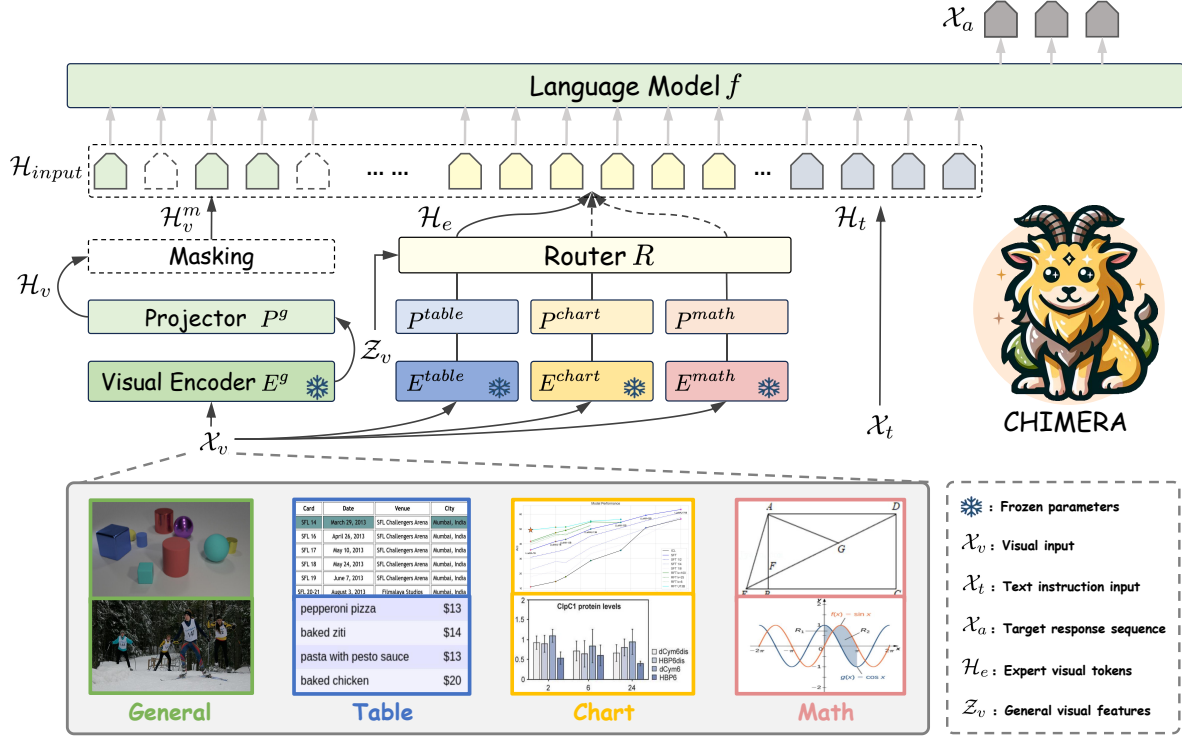


Figure 2. **Overview of our Chimera framework.** Chimera uses Generalist-Specialist Collaboration Masking to facilitate the alignment with expert models. During inference, the Router  $R$  decides expert invocations based on the visual input, resulting in a versatile model that excels across multiple specialized domains and tasks.

reduce generalizability, leading to trade-offs or suboptimal performance across subtasks. The latter approach incorporates encoded features from various domains, but applying this directly to a well-aligned LMM may lead to misalignment between the generalist and specialist models—a limitation we will discuss in the next section.

### 3.3. Generalist-Specialist Collaboration Masking

Although naive concat method with input  $\mathcal{H}_{input}^{nc}$  is intuitive, we still concern that since the general visual encoder  $E^g$  is well-aligned with language Model  $f$ , it may cause the model to overly rely on  $E^g$  to complete tasks, which leads to ineffective alignment with the expert models. To better align domain knowledge and general world knowledge, we propose a simple yet effective learning mechanism called Generalist-Specialist Collaboration Masking, designed to boost the synergy between general-purpose and domain-specific capabilities.

During training, we sample a subset of general visual tokens from  $\mathcal{H}_v$  at a certain ratio and mask them to build the masked general visual tokens  $\mathcal{H}_v^m$ . In practice, this is achieved by setting the attention mask corresponding to the sampled subset to False. We consider a simple sampling strategy: randomly sampling tokens without replacement according to a uniform distribution. Applying mask to information provided by general encoder  $E^g$  produces a limi-

tation on  $E^g$ , which will force the model to utilize domain-specific information provided by expert models as supplements for vision-language tasks. The uniform distribution helps prevent bias that may arise from masking predominantly in the image center or specific regions.

### 3.4. Training Recipe

To equip multi-modal generalists with rich domain-specific knowledge, we apply a progressive training strategy, including Domain-General Knowledge Alignment and Visual Instruction Tuning. Through two-stage training, we develop variants for different scenarios respectively. All the datasets used are publicly available. Details about the datasets can be found in the supplementary material.

**Domain-General Knowledge Alignment.** To initially align domain-specific knowledge with the semantic space of the generalist LMM, we train the model using tasks that directly perceive diverse image content. The tasks include natural image description, table format transformation, chart structural extraction and summarization, math diagram captioning, and paragraph-level OCR.

With guidance from image-text pairs across different domains, the model is able to leverage domain knowledge from expert models to accurately recognize visual content in each domain and describe its spatial arrangement. This marks the first step toward deeper integration. In this stage,



we freeze the general visual encoder  $E^g$ , expert model set  $S^e$  and language model  $f$ , only train the router  $R$ , general projector  $P^g$  and expert projector set  $S^p$ .

**Visual Instruction Tuning.** To further align model with domain knowledge from expert models and enhance its performance on specialized tasks across different domains, we take instruction-following datasets from various domains to perform visual instruction tuning with the proposed GSCM. During this stage, we unfreeze router  $R$ , general projector  $P^g$ , expert projector set  $S^p$  and language model  $f$ , perform a thorough instruction-following tuning, which finally results in the versatile Chimera models.

**Training Objective.** Our primary training objective is to optimize the trainable parameters  $\theta$ , so that the likelihood of target response sequence  $\mathcal{X}_a$  is maximized given the visual input  $\mathcal{X}_v$  and instruction  $\mathcal{X}_t$  as follows:

$$\theta^* = \arg \max_{\theta} P(\mathcal{X}_a | \mathcal{X}_v, \mathcal{X}_t; \theta). \quad (5)$$

To accomplish this, we utilize token-wise cross-entropy loss to train the model in an auto-regressive manner. For target  $\mathcal{X}_a$  of length  $L$ , the auto-regressive modeling loss  $\mathcal{L}_m$  is represented as follows:

$$\mathcal{L}_m = - \sum_{i=1}^L \log P(x_i | \mathcal{X}_v, \mathcal{X}_t, \mathcal{X}_{a;<i}, \theta), \quad (6)$$

where  $\mathcal{X}_{a;<i}$  are the tokens before the current prediction token  $x_i$ .

Besides, we add classification loss to guide the Router to accurately call different expert models based on image content, which can be represented as follows:

$$\mathcal{L}_c = - \sum_{i=0}^{N_e+1} \log P(c_i | \mathcal{X}_v, \theta), \quad (7)$$

where  $c_i$  represents the expert domain category that the current image requires for invocation (including category 0, which means no expert model is invoked). Finally, the optimization objective is formulated as follows:

$$\mathcal{L} = \mathcal{L}_c + \mathcal{L}_m. \quad (8)$$

## 4. Experiments

To evaluate the capabilities of Chimera, we begin by detailing the datasets and metrics used for evaluation, along with the implementations for multi-modal reasoning and visual content extraction in Sec. 4.1. Then, we provide a comparison of Chimera models against previous generalist models across various benchmarks, including multi-modal reasoning (Sec. 4.2) and visual structural extraction (Sec. 4.3). Besides, we conduct further analysis on the model design and training strategy in Sec. 4.4.

### 4.1. Datasets, Metrics and Implementation Details

**Datasets.** In this paper, we conduct quantitative evaluations of Chimera model across a range of challenging multi-modal benchmarks, categorized into the following areas:

- **Multi-modal Reasoning.** We evaluate the Chimera on the MathVista [48] to determine its visual reasoning capabilities. Besides, we extend our evaluation on the MathVerse [90], which is specifically designed for mathematical problem-solving, to gauge its performance in multi-modal mathematical reasoning.
- **Visual Structural Extraction (SE).** Evaluations of Chimera on chart domain are conducted on the challenging ChartQA-SE [52] and PlotQA-SE [84] benchmarks. Following the protocol of StructChart [81], we utilize the test sets of both the ChartQA [52] and PlotQA [57] to ensure a fair comparison. For table and document, we manually collected and annotated a table format transformation benchmark called Table-SE and a document structural extraction benchmark called Doc-SE. Details regarding the data collection and annotation process can be found in the supplementary material.

**Metrics.** In evaluations, we adhere to the default metrics used by benchmarks, such as MathVista, MathVerse, ChartQA-SE, and PlotQA-SE. For the assessment of the table format transformation, we use Tree-EditDistance-based Similarity (TEDS) score and Edit Distance for evaluation. For document structural extraction, we take Edit Distance, Precision, BLEU and METEOR as evaluation metrics.

**Implementation Details.** We initialize Chimera using the InternVL2 series. Specifically, we use InternVL2-2B, 4B, 8B to construct Chimera-2B, 4B, and 8B for multi-modal reasoning, while using InternVL-1B to build Chimera for visual content extraction. In each training phase, we train the model for one epoch on the public datasets (refer to supplementary materials for more details). For multi-modal reasoning scenario, we take StructEqTable [83], ChartVLM [84] and Math-CLIP [89] as table, chart and math expert respectively. For visual content extraction scenario, we employ GOT [80] as the document expert. More detailed implementation specifics can be found in the supplementary material.

### 4.2. Comparison on Multi-modal Reasoning

**Comparison with Generalist Models.** LMMs, such as LLaVA-OneVision [30], Qwen2-VL [77], InternVL2 [12] and GPT-4o demonstrate powerful multi-modal reasoning abilities on general purpose scenarios. However, these generalist models always exhibit limited performance when handling tasks under professional scenarios. Our model demonstrates exceptional performance on the challenging multi-modal reasoning benchmarks MathVista and MathVerse, significantly outperforming existing generalist models. As shown in Tab. 1 and Tab. 2, Chimera-8B achieved overall accuracies of 64.9 and 32.4, respectively, setting

Model	#Params.	ALL	FQA	GPS	MWP	TQA	VQA	ALG	ARI	GEO	LOG	NUM	SCI	STA
<i>Close Source LLMs</i>														
InternVL2-Pro [12]	-	66.8	70.6	65.4	76.9	71.5	48.0	66.5	62.3	63.6	27.0	40.3	65.6	81.1
Gemini 1.5 Pro [70]	-	63.9	-	-	-	-	-	-	-	-	-	-	-	-
GPT-4o	-	63.8	-	-	-	-	-	-	-	-	-	-	-	-
Grok-1.5V	-	52.8	-	-	-	-	-	-	-	-	-	-	-	-
Claude 3 Opus [1]	-	50.5	-	-	-	-	-	-	-	-	-	-	-	-
GPT-4V (Playground)	-	49.9	43.1	50.5	57.5	65.2	38.0	53.0	49.0	51.0	21.6	20.1	63.1	55.8
<i>Open Source LLMs</i>														
LLaVA-OneVision [30]	72B	67.5	-	-	-	-	-	-	-	-	-	-	-	-
Math-LLaVA* [67]	13B	46.6	37.2	57.7	56.5	51.3	33.5	53.0	40.2	56.5	16.2	33.3	49.2	43.9
Pixtral [2]	12B	58.0	-	-	-	-	-	-	-	-	-	-	-	-
SPHINX-MoE [40]	8×7B	42.7	-	-	-	-	-	-	-	-	-	-	-	-
InternLM-XComposer2 [15]	7B	57.6	55.0	63.0	<b>73.7</b>	56.3	39.7	56.6	52.4	62.3	8.1	42.4	59.0	64.1
LLaVA-OneVision [30]	7B	63.2	-	-	-	-	-	-	-	-	-	-	-	-
Math-PUMA-DeepSeek-Math* [93]	7B	44.7	42.8	39.9	67.7	42.4	31.3	39.2	41.9	41.4	8.1	36.8	48.4	52.5
Qwen2-VL [77]	2B	43.0	-	-	-	-	-	-	-	-	-	-	-	-
	7B	58.2	-	-	-	-	-	-	-	-	-	-	-	-
InternVL2 [12]	2B	48.3	51.3	45.7	40.9	50.6	52.5	43.4	47.3	42.3	13.5	28.5	53.3	56.8
	4B	57.0	58.0	58.2	62.4	57.0	48.6	55.9	53.8	55.2	13.5	30.6	59.0	65.1
	8B	61.6	62.5	64.4	61.3	64.6	<b>54.7</b>	63.0	<b>58.9</b>	61.9	18.9	34.0	59.0	70.1
Chimera	2B	53.1	52.4	56.7	62.9	51.9	40.8	52.7	47.6	56.1	10.8	34.0	52.5	61.1
	4B	61.3	58.4	66.8	72.0	61.4	48.0	63.3	54.7	65.7	<b>24.3</b>	39.6	60.7	66.4
	8B	<b>64.9</b>	<b>62.8</b>	<b>71.6</b>	72.6	<b>65.2</b>	52.0	<b>67.6</b>	57.8	<b>69.5</b>	21.6	<b>45.8</b>	<b>61.5</b>	<b>69.4</b>
<i>LLMs with Preference Optimization</i>														
InternVL-MPO [79]	8B	67.3	<b>72.5</b>	73.6	69.9	<b>66.5</b>	50.3	70.1	57.5	71.5	27.0	43.1	65.6	79.1
Ovis1.6-Gemma2 [50]	9B	67.2	-	-	-	-	-	-	-	-	-	-	-	-
Chimera <sup>†</sup>	8B	<b>68.3</b>	66.5	<b>76.9</b>	<b>80.1</b>	60.8	<b>55.3</b>	<b>69.7</b>	<b>64.8</b>	<b>74.5</b>	13.5	<b>49.3</b>	<b>62.2</b>	<b>77.7</b>
Human performance	-	60.3	59.7	48.4	73.0	63.2	55.9	50.9	59.2	51.4	40.7	53.8	64.9	63.9

Table 1. Accuracy scores on the *testmini* subset of MathVista. Task types: FQA: figure QA, GPS: geometry problem solving, MWP: math word problem, TQA: textbook QA, VQA: visual QA. Math reasoning types: ALG: algebraic, ARI: arithmetic, GEO: geometry, LOG: logical, NUM: numeric, SCI: scientific, STA: statistical. Chimera<sup>†</sup> represents post-trained Chimera model. \* represents the domain expert model. Chimera set a new SOTA results of 64.9 among open source LLMs under 70B scale. Direct preference optimization further boost Chimera’s performance to 68.3, outperforming the latest LLMs with preference optimization.

a new state-of-the-art (SOTA) for LLMs under the 70B scale. Chimera-2B and Chimera-4B both significantly outperform the baseline InternVL2 series and achieve results comparable to models of much larger scales. On MathVista, Chimera-8B stands out among both closed-source and open-source LLMs of the same size, leading GPT-4o by 1.1%, and outperforming Qwen2-VL and InternVL by 6.7% and 3.9%, respectively. On MathVerse, Chimera-8B is only slightly behind GPT-4V, and surpasses the hundred-billion-scale LLaVA-NeXT by 7.9 points. This demonstrates that our approach, by integrating domain knowledge from different expert models, effectively enhances performance in specialized domains.

**Comparison with Specialist Models.** Compared to specialist models such as Math-LLaVA [67], Math-PUMA [93], MAVIS [89], and GeoX [82], Chimera demonstrates outstanding performance. As reported in Tab. 1 and Tab. 2, Chimera-8B outperforms the previous best expert models by 18.3% and 4.9% on MathVista and MathVerse,

respectively. In contrast, the latest expert model, Math-PUMA [93], achieves performances of 44.7 and 31.8 on the two benchmarks, which is notably inferior to our method. It is worth noting that these expert models have limited generalization ability and cannot handle tasks from other domains. In contrast, our model excels across various tasks in the table, chart, and document domains, proving Chimera’s powerful versatility.

**Further Improve Reasoning Ability with Preference Optimization.** The emergence of preference optimization like RLHF has revolutionized model enhancement strategies. Chimera is able to capitalize on this trend through seamless preference optimization training integration, demonstrating remarkable scalability. We construct 60K preference pairs using publicly available datasets and Chimera’s outputs and perform a naive Direct Preference Optimization to develop Chimera<sup>†</sup>. Specific data construction process can be found in the supplementary material. Chimera<sup>†</sup>, with naive post-train, surpasses SOTA post-training methods by

Model	#Params.	All Acc	Text Dominant	Text Lite	Vision Intensive	Vision Dominant	Vision Only
<i>Closed-source MLLMs</i>							
Gemini-Pro [69]	-	23.5	26.3	23.5	23.0	22.3	22.2
Qwen-VL-Max [5]	-	25.3	30.7	26.1	24.1	24.1	21.4
GPT-4V	-	39.4	54.7	41.4	34.9	34.4	31.6
<i>Open-source MLLMs</i>							
SPHINX-Plus [40]	13B	14.0	16.3	12.8	12.9	14.7	13.2
SPHINX-MoE [40]	8×7B	15.0	22.2	16.4	14.8	12.6	9.1
LLaVA-NeXT [29]	110B	24.5	31.7	24.1	24.0	22.1	<b>20.7</b>
LLaVA-NeXT [29]	8B	19.3	24.9	20.9	20.8	16.1	13.8
InternLM-XComposer2 [15]	7B	16.5	22.3	17.0	15.7	16.4	11.0
Math-LLaVA* [67]	13B	19.0	21.2	19.8	20.2	17.6	16.4
MAVIS-7B* [89]	7B	27.5	41.4	29.1	27.4	24.9	14.6
Math-PUMA-DeepSeek-Math* [93]	7B	31.8	<b>43.4</b>	35.4	33.6	31.6	14.7
InternVL2 [12]	2B	21.4	24.1	22.5	22.8	21.1	16.6
	4B	26.3	32.0	28.6	28.0	24.4	18.8
	8B	31.3	38.8	34.5	33.6	32.6	17.0
Chimera	2B	22.6	27.3	23.9	22.3	22.8	16.9
	4B	27.2	31.4	30.8	29.7	25.7	18.2
	8B	<b>32.4</b>	39.6	<b>35.8</b>	<b>34.8</b>	<b>32.7</b>	19.3

Table 2. Performance Comparison on MathVerse with the accuracy metric. \* represents the domain expert model.

Model	ALL	General	Chart	Table	Math
InternVL2-2B [12]	48.3	45.3	58.9	50.0	44.2
InternVL2-4B [12]	57.0	50.1	66.2	65.7	58.3
InternVL2-8B [12]	61.6	52.7	<b>71.2</b>	67.1	66.5
Chimera-2B	53.1	46.0	60.3	62.9	56.1
Chimera-4B	61.3	54.0	64.8	<b>72.9</b>	66.9
Chimera-8B	<b>64.9</b>	<b>57.5</b>	<b>71.2</b>	62.9	<b>71.9</b>

Table 3. Accuracy scores of different visual content domain on the *testmini* subset of MathVista. Those do not belong to the last three domains are uniformly classified as General for simplicity.

1.0%, shows significant 3.4% improvement over base models without post-training, highlighting the framework’s scalability and potential.

**Fine-Grained Analysis.** We manually classified MathVista questions by the domain of visual content and present the model’s performance across domains in Tab. 3. In most cases, the model outperforms its baseline in each domain, further demonstrating that incorporating expert models enhances the generalist model’s performance on specialized tasks. We also observed that expert models improve performance in general scenarios, suggesting that domain knowledge provides diverse insights for language model in handling visual information, thereby enhancing the model even on scenarios where experts are not activated.

Chimera-8B performs similarly in the chart domain but slightly worse in the table domain. This is due to the over-specialized function of the table expert, which, despite sup-

porting comprehensive extraction, may introduces noise for the 8B baseline model because of the considerable task gap. In contrast, the chart expert’s pre-training task covers both extraction and perception, with minimal impact. The math expert consistently improves performance across models due to its alignment with reasoning tasks.

### 4.3. Comparison on Visual Structural Extraction

**Comparison with Generalist Models.** For specialized tasks beyond VQA, generalist models similarly show limited performance. Tab. 4 and Tab. 5 present the results of visual structural extraction in the Chart and Table domains, respectively. On ChartQA-SE and PlotQA-SE, Chimera outperforms representative generalist models such as GPT-4V, Qwen-VL [5], and InternVL-2 [12] across the AP@strict, AP@slight, and AP@high metrics. In Table-SE, Chimera leads InternVL2 and Qwen2-VL by a larger margin in Edit Distance and TED scores, demonstrating strong domain-specific capability.

Tab. 6 and Fig. 3 exhibit results on Doc-SE, Chimera significantly outperforms InternVL2 [12] across four metrics in bilingual tasks and shows balanced performance across different document categories.

**Comparison with Specialist Models.** Compared to specialist models majoring in single task, Chimera still demonstrates strong performance. Specifically, for ChartQA-SE and PlotQA-SE, Chimera achieves excellent or competitive results across three metrics compared to the SOTA expert model GOT. In Table-SE, Chimera also achieves comparable TED scores and outperforms with a lower Edit Distance

Task	Metric	Deplot* [42]	UniChart* [53]	ChartVLM* [84]	GPT-4V	Qwen-VL [5]	GOT [80]	InternVL-2 [12]	Chimera
ChartQA-SE	AP@strict	61.4	42.3	71.8	50.4	58.6	<b>74.7</b>	73.7	74.1
	AP@slight	70.9	53.1	81.4	60.6	68.5	<b>84.5</b>	83.9	84.4
	AP@high	72.9	56.0	84.2	64.3	72.7	86.7	87.2	<b>87.6</b>
PlotQA-SE	AP@strict	3.1	10.5	3.8	7.3	0.5	<b>13.3</b>	5.7	5.9
	AP@slight	16.5	26.0	46.8	19.4	4.2	59.6	55.0	<b>62.1</b>
	AP@high	26.5	26.9	54.0	22.3	12.0	64.0	61.8	<b>71.0</b>

Table 4. Performance on ChartQA-SE and PlotQA-SE. Metrics include Average Precision (AP) at strict, slight, and high levels. \* represents the domain expert model.

Method	Edit Distance↓	TEDS↑	TEDS (structure only)↑
InternVL-2 [12]	0.229	0.676	0.762
Qwen2-VL [77]	0.231	0.690	0.773
StructEqTable* [83]	0.226	0.706	0.787
GOT* [80]	0.257	<b>0.745</b>	<b>0.830</b>
Chimera	<b>0.165</b>	0.740	0.828

Table 5. Comparison of performance on Table-SE across different methods: TEDS, TEDS (structure only), and Edit Distance. \* represents the domain expert model.

Method	Edit Distance↓		Precision↑		BLEU↑		METEOR↑	
	en	zh	en	zh	en	zh	en	zh
InternVL [12]	0.504	0.604	65.4	66.0	38.4	33.1	52.6	50.6
GOT* [80]	0.355	0.510	67.9	<b>71.2</b>	<b>52.5</b>	34.3	<b>65.3</b>	53.9
Chimera	<b>0.304</b>	<b>0.461</b>	<b>69.6</b>	66.1	49.8	<b>40.5</b>	64.8	<b>56.9</b>

Table 6. Comparison of performance metrics across different methods on Doc-SE. Metrics include Edit Distance (lower is better), Precision, BLEU, and METEOR (higher is better). \* represents the domain expert model.

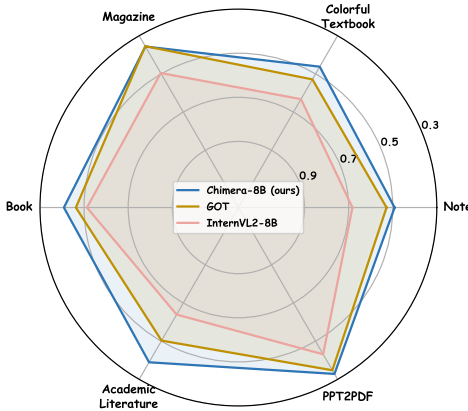


Figure 3. Comparison of Edit Distance ↓ across different document categories on Document Structural Extraction (Doc-SE) task.

by 0.092. As for Doc-SE, Chimera leads in most metrics for both English and Chinese documents, showing better overall generalization across document categories than GOT.

#### 4.4. Further analysis

**Effects of GSCM.** To assess whether our proposed GSCM enhances alignment with the expert model, we analyze the attention distribution of the model’s output across general

GT \ Prediction	General	Table	Chart	Math
<b>General</b>	–	0	16	6
<b>Table</b>	1	–	0	0
<b>Chart</b>	1	0	–	0
<b>Math</b>	22	0	0	–

Table 7. Error statistics of router on MathVista *testmini*.

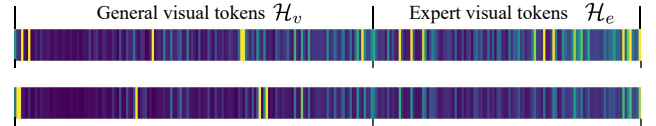


Figure 4. Attention distribution on Chimera with (Top) & without (Bottom) masking.

visual tokens  $\mathcal{H}_v$  and expert visual tokens  $\mathcal{H}_e$ . As illustrated in Fig. 4, Chimera places greater emphasis on domain features during inference, demonstrating improved alignment between the specialist models and the generalist LMM. In contrast, Chimera w/o masking exhibits significantly weaker utilization of domain features. This occurs because the general encoder, which is already well-aligned with the language model, often results in imbalanced optimization between the general encoder and expert models.

**Analysis about Expert Router Error.** Due to the significant differences in visual inputs across different domains, Chimera can achieve effective classification using a simple linear layer, thereby guiding expert model selection. As shown in Tab. 7, it achieves 95.4% accuracy on MathVista, proving the router’s effectiveness. All errors stem from confusion between the general and expert domains, not between experts. This issue arises because training labels are dataset-based, and the “general” category includes mixed-domain images. Explicit domain annotation for each image could better address this.

## 5. Conclusion

We present Chimera, a scalable pipeline that integrates specialist models into generalist LMMs, enabling adaptation to specialized tasks. Our approach transforms LMMs, like InternVL-2, into versatile models capable of handling tasks across tables, math, documents, *etc.* Chimera pioneers new directions for bridging generalist and specialist models.



## **Acknowledgements**

The research was supported by Shanghai Artificial Intelligence Laboratory, a locally commissioned task from the Shanghai Municipal Government, the Shanghai Municipal Science and Technology Major Project, and Shanghai Rising Star Program (Grant No. 23QD1401000).

This work is supported by National Key Research and Development Program of China (No. 2022ZD0160101), Shanghai Natural Science Foundation (No. 23ZR1402900), Shanghai Municipal Science and Technology Major Project (No.2021SHZDZX0103). The computations in this research were performed using the CFFF platform of Fudan University.



# Chimera: Improving Generalist Model with Domain-Specific Experts

## Supplementary Material

Due to the eight-page limitation of the main text, we provide more details and visualizations from the following aspects:

- Sec. 6: Selection strategy for pre-training tasks and expert models.
- Sec. 7: Dataset Details in training.
- Sec. 8: Chimera’s performance on general tasks.
- Sec. 9: Details about preference optimization.
- Sec. 10: Experiment results on mask ratio selection.
- Sec. 11: Introduction of Table-SE and Doc-SE.
- Sec. 12: Experiments of scaling up more experts.
- Sec. 13: Comparison with existing works.
- Sec. 14: More information of implementation details.
- Sec. 15: Visualization of Chimera’s visual content extraction performance.

## 6. Pre-training Tasks and Expert Models

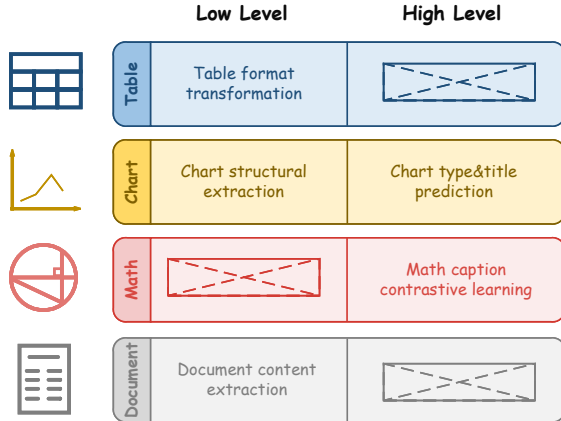


Figure 5. Pre-training tasks of expert models considered by Chimera.

The type of pre-training task significantly affects model performance, which we consider when selecting expert models. As shown in Fig. 5, we categorize low-level tasks as the precise extraction of domain-specific visual content and structure (*e.g.*, Table2LaTeX, Chart2Markdown, Doc2Markdown), while high-level tasks involve understanding and summarizing image content. We select expert models with diverse pre-training task configurations. For the table expert, we use the encoder from StructE-qTable [83], which effectively converts table images into LaTeX/HTML. For the chart expert, we choose the encoder from ChartVLM [84], which excels in structural extraction and chart type classification. For the math expert, we adopt Math-CLIP [89], trained on extensive geometry and func-

Stage 1	<b>General:</b> ShareGPT4v [10], ShareGPT4-o [10]
	<b>Table:</b> TableX [83]
	<b>Chart:</b> ChartQA [52], PlotQA [57], ChartX [84], SimChart [81]
	<b>Math:</b> MAVIS-Caption [89]
Stage 2:	<b>Language:</b> Kaggle-science-exam [38], MathInstruct [87], MathQA [3], SciInstruct [88], Orcamath [58]
	<b>General:</b> ShareGPT4v [10], ShareGPT4-o [10], LLaVAR [91], AI2D (GPT4V) [30], AI2D (InternVL [12]), AI2D (Original) [27], MathVision [76], IconQA [47], MapQA [8], ScienceQA [63], ArxivQA [33], TQA [28], CLEVR-Math [21], Super-CLEVR [36], Cambrian Data Engine [72]
	<b>Table:</b> TableX [83], TabMWP [49], MMTab [92]
	<b>Chart:</b> PlotQA [57], ChartX [84], SimChart [81], Chart2Text [25], ChartQA [52], LRV Chart [43], ChartGemma [55], DVQA [23], FigureQA [24], VisText [68]
	<b>Math:</b> MAVIS-Caption [89], Geo170K [17], GeoMVerse [26], MAVIS Manual Collection [89], MAVIS Data Engine [89], Geometry3K [46], GeoQA+ [9], InterGPS [46]

Table 8. Dataset used for multi-modal reasoning scenario. **Stage 1** and **Stage 2** represent Domain-General Knowledge Alignment and Visual Instruction Tuning separately.

Stage 1	ChartQA [52], PlotQA [57], ChartX [84], SimChart [81], TableX [83]
Stage 2	DocGenome [83], DocStruct4M [19], DocVQA [56]

Table 9. Datasets used for visual content extraction scenario. **Stage 1** represents Domain-General Knowledge Alignment, and **Stage 2** represents Visual Instruction Tuning.

tion caption data. For document structural extraction, we employ the encoder from the latest model, GOT [80].

## 7. Dataset Details

The datasets used for Chimera is presented in Tab. 8 and Tab. 9. All the datasets we used come from publicly accessible datasets.

## 8. Evaluation on General Tasks

We evaluate Chimera’s general capabilities using the perception set from the general benchmark MME [16], with results presented in Tab. 10. Across different model sizes, Chimera and InternVL exhibit varying strengths across different tasks, achieving overall comparable performance.

	InternVL2		Chimera	
	4B	8B	4B	8B
<b>Existence</b>	200.00	190.00	200.00	195.00
<b>Count</b>	123.33	158.33	130.00	155.00
<b>Position</b>	143.33	155.00	123.33	148.33
<b>Color</b>	165.00	175.00	160.00	190.00
<b>Posters</b>	158.84	168.03	159.86	164.97
<b>Celebrity</b>	125.00	148.53	145.29	162.65
<b>Scene</b>	158.75	152.50	163.50	157.75
<b>Landmark</b>	167.25	178.25	167.25	177.75
<b>Artwork</b>	144.75	154.50	144.00	153.00
<b>OCR</b>	147.50	162.50	117.50	132.50

Table 10. Performance on perception sub-tasks of MME.

This suggests that the Chimera framework introduces minimal degradation to the model’s general task capabilities. Meanwhile, Chimera demonstrates strong expertise in domains such as tables, math, charts, and documents, further validating that our proposed approach effectively enhances a generalist LMM’s domain-specific knowledge without compromising its general performance.

## 9. Details about preference optimization

For preference optimization, we adopt a commonly used approach: we randomly sample 10k problems from MathV-360K, generating 16 responses per problem using Chimera. Each response is classified based on correctness using rule-based answer matching, and after filtering, we construct 60k preference pairs for Direct Preference Optimization (DPO) training. Then we perform DPO training on 60K data for 1 epoch.

## 10. Mask Ratio Selection

Model	Ratio	ALL	General	Chart	Table	Math
InternVL2-4B [12]	N/A	57.0	50.1	66.2	65.7	58.3
InternVL2-4B-NF [12]	N/A	58.5	51.5	67.1	<b>74.3</b>	58.6
Chimera-4B-0.0	0.0	59.4	50.8	66.2	67.1	65.5
Chimera-4B	0.3	<b>61.3</b>	<b>54.0</b>	64.8	72.9	<b>66.9</b>
Chimera-4B-0.5	0.5	60.4	51.3	<b>68.5</b>	70.0	65.8
Chimera-4B-1.0	1.0	56.2	51.5	63.5	72.9	53.6

Table 11. Ablation results on different visual content domain on the *testmini* subset of MathVista. InternVL2-4B-NF represents naive finetune of baseline with same settings, Chimera-4B-*R* means Chimera model trained with mask ratio *R* in GSCM.

We conducted an ablation study on 4B scale models to assess our approach’s effectiveness, as shown in Table 11. It should be noted that model with mask ratio 1.0 does not have access to the general encoder during training, contrary to our intentions. Thus, we modified this case to give the model an 80% probability of masking all general features. The results show that naively finetuning the LMM leads to limited performance improvement. By incorporat-

ing domain knowledge from expert models, even the case without GSCM still yields better results than naive finetuning. As the mask ratio increases, the model’s performance improves initially and then declines. This indicates that slightly masking helps balance encoder optimization, leading to better alignment. However, as the mask ratio increase, we believe excessive masking prevents the model from effectively learning to utilize both features for reasoning. Based on the above observations, we set the mask ratio to 0.3 in Chimera’s implementation. We also observed that performance trends vary across domains as the mask ratio changes, suggesting that the alignment difficulty of expert models differs by domain and task, which we leave for future exploration.

## 11. Details of Table-SE and Doc-SE

In Tables 7 and 8 of the main text, we conduct the experiments on Table Structural Extraction (Table-SE) task and Document Structural Extraction (Doc-SE) task, respectively. In this section, we primarily introduce the evaluation dataset construction method and provide detailed information about the dataset.

### 11.1. Data Source

	Count
<b>Document Categories</b>	
PPT2PDF	43
Academic Literature	42
Book	13
Colorful Textbook	37
Magazine	30
Exam Paper	7
Note	18
Newspaper	15
<b>Language</b>	
Simplified Chinese	128
English	77
<b>Layout</b>	
1 and More Column	27
Single Column	91
Other Layout	43
Double Column	40
Three Column	4
# Total	205

Table 12. Statistical information of Doc-SE.

Our benchmark was developed through a systematic sampling process from an initial collection of 200,000 PDF documents sourced from Common Crawl, Google, Baidu search engines, and internal repositories. We initially extracted visual features using ResNet-50 [18] and performed clustering algorithm using Faiss [22] to identify diverse document patterns. From the 10 cluster centers, we sampled 6,000 visually diverse pages, which were then manu-

	Count
<b>Background</b>	
w/o Background	80
w/ Background	20
<b>Equation</b>	
w/o Equation	78
w/ Equation	22
<b>Language</b>	
English	45
English & Chinese Mixed	5
Chinese	50
<b>Table Format</b>	
Three-line Table	47
Full-bordered Table	39
Partial-bordered Table	14
w/o Merged Cells	58
w/ Merged Cells	42
<b>Layout</b>	
Horizontal	97
Vertical	3
# Total	100

Table 13. Statistical information of Table-SE.

ally annotated with attributes such as page type, layout type, and language. As illustrated in Table 12 and Table 13, the final benchmark includes 205 page-level PDF images and 100 table images, ensuring comprehensive representation of real-world document scenarios with various layouts and attributes.

### 11.2. Annotation Process

For ensuring annotation quality and efficiency, we design separate standardized processes for page-level PDF documents and tables.

For page-level PDF documents, our process consists of three stages: (1) We first employ fine-tuned LayoutLMv3 for layout detection and PaddleOCR for text recognition as intelligent pre-annotation. (2) Professional annotators then refine the detection boxes, verify text content accuracy, and enhance annotations with reading order and affiliation details. (3) Finally, researchers review the annotations to ensure overall quality and accuracy.

For table annotations, we follow a similar but specialized three-stage approach: (1) We utilize GPT-4o and PaddleOCR for initial table annotations. (2) Annotators then verify and correct the table structure and content, using specialized tools like Tables Generator for verification. (3) Finally, experts through table annotations re-rendering to ensure correct HTML and LaTeX code labels.

### 11.3. Showcase

We provide several visualization examples of Table-SE in Fig. 6 and Fig. 7, where each item contains a visual table and its corresponding LaTeX code.

## 12. Experiments of Scaling Up More Experts

Model	ALL	General	Chart	Table	Math
InternVL2-4B	57.0	50.1	66.2	65.7	58.3
InternVL2-4B w/ Chart Expert	59.4	52.0	68.0	72.9	60.8
Chimera-4B	61.3	54.0	64.8	72.9	66.9

Table 14. Accuracy scores of different visual content domain on the *testmini* subset of MathVista. Those do not belong to the last three domains are uniformly classified as General for simplicity. InternVL2-4B w/ Chart Expert represent the case only integrating chart expert model.

To further validate the impact of scaling up the number of expert models, we provide ablation results introducing only the chart expert. In this case, non-chart data is encoded solely by the general encoder during training. As shown in Table 14, incorporating only the chart expert obtains lower MathVista [48] overall score by 1.9 points than Chimera-4B.

Specifically, InternVL2-4B w/ Chart Expert also shows improvements in general scenarios, though less significant than Chimera, which integrates three expert models. In the chart domain, InternVL2-4B w/ Chart Expert achieves notable gains by avoiding conflicts among multiple experts with large task gaps. However, Chimera’s integration of multiple experts enhances performance across diverse domains, boosting overall results. In the math domain, InternVL2-4B w/ Chart Expert scores 6.1 points lower than Chimera, demonstrating the strong mathematical reasoning capabilities derived from integrating the math expert.

## 13. Comparison with existing works

Integrating specialist experts that contain specialized prior knowledge presents a promising approach to improve the specific capabilities of generalist model. MoVA [94] proposes a multi-turn method that relies on the language model to call an expert in the first round and generates responses in the second, which reduces conciseness and efficiency. MoME [66] uses soft-weighting to fuse multiple visual encoders, enabling VLMs to benefit from leveraging representations from different encoders. However, this approach lacks explicit guidance for encoder selection and introduces additional concerns such as inference efficiency and uniform visual feature sizes.

## 14. Training Configuration

The training strategy is summarized in Tab 15 and Tab 16. During the two-stage training process, we gradually increase the maximum image resolution and the number of visual tokens of the general visual encoder  $E^g$ . In the Domain-General Knowledge Alignment stage, we use



## Visual Table

	Beef meat				Chicken meat				Pork meat			
	Cases	Controls	OR	95% CI	Cases	Controls	OR	95% CI	Cases	Controls	OR	95% CI
Never Exposed (Ref group)	1,823	2,273	1.00		1,823	2,273	1.00		1,823	2,273	1.00	
Ever Exposed	117	108	1.22	0.90-1.67	136	129	1.19	0.91-1.55	145	143	1.09	0.83-1.42
Duration of exposure												
<5 years	40	37	1.45	0.92-2.31	30	40	0.97	0.60-1.58	39	41	1.25	0.80-1.96
6-15 years	29	43	0.79	0.47-1.31	42	41	1.21	0.78-1.88	44	58	0.84	0.55-1.28
>16 years	48	28	1.63	0.95-2.88	64	48	1.36	0.90-2.06	61	43	1.28	0.81-2.03
p-value of test for linear trend (with ref cat)			0.23				0.11				0.54	
Intensity of exposure												
Low	60	59	1.26	0.86-1.83	71	68	1.24	0.88-1.75	70	72	1.15	0.82-1.62
Medium	42	35	1.22	0.73-2.04	47	46	1.11	0.72-1.71	55	52	1.03	0.68-1.58
High	15	14	0.91	0.35-2.40	18	15	1.22	0.56-2.65	20	19	0.89	0.40-1.94
p-value of test for linear trend (with ref cat)			0.36				0.29				0.78	

**Table 1. Anticonvulsant activity and protective index of intraperitoneal AEDs in mice**

AED	Rofenol test		MES test		Phenytoin test		Bicuculline		Picrotoxin		Strychnine	
	TD <sub>50</sub> (95% CI)	PI	ED <sub>50</sub> (95% CI)	PI	ED <sub>50</sub> (95% CI)	PI	ED <sub>50</sub> (95% CI)	PI	ED <sub>50</sub> (95% CI)	PI	ED <sub>50</sub> (95% CI)	PI
Rofenol	15.1 (12.5-18.1)	23.2	54.0 (40.0-72.1)	9.9	76.3 (60.0-96.0)	9.9	76.3 (60.0-96.0)	9.9	76.3 (60.0-96.0)	9.9	76.3 (60.0-96.0)	9.9
Phenobarbital	65.5 (52.2-72.1)	4.9	13.2 (5.9-15.9)	5.2	37.7 (26.5-47.4)	1.8	27.5 (20.8-34.8)	2.5	55.1 (40.8-72.1)	0.7	95.3 (71.3-99.5)	0.7
Phenytoin	69.0 (62.8-72.9)	3.2	18.6 (12.2-25.7)	2.9	45.9 (35.9-59.0)	1.2	59.7 (31.1-144.0)	1.1	29.2 (26.1-32.3)	1.5	29.2 (26.1-32.3)	1.5
Valproate	442.8 (381-460)	1.4	12.3 (1.1-15.1)	2.4	45.9 (35.9-59.0)	1.2	59.7 (31.1-144.0)	1.1	29.2 (26.1-32.3)	1.5	29.2 (26.1-32.3)	1.5
Carbamazepine	442.8 (381-460)	1.4	12.3 (1.1-15.1)	2.4	45.9 (35.9-59.0)	1.2	59.7 (31.1-144.0)	1.1	29.2 (26.1-32.3)	1.5	29.2 (26.1-32.3)	1.5
Maximum protection, 37.5%												
Maximum protection, 50.0%												
Maximum protection, 62.5%												

AED, antiepileptic drug; MES, maximal electroshock; TD<sub>50</sub>, the dose eliciting evidence of minimal neurotoxicity in 50% of animals; CI, confidence interval; ED<sub>50</sub>, the dose of drug required to produce the desired end point in 50% of animals; and PI, protective index (ratio of TD<sub>50</sub> to ED<sub>50</sub>).

## Ground Truth: LaTeX

```

\begin{tabular}{c}
\hline
\multicolumn{4}{c}{Beef meat} & \multicolumn{4}{c}{Chicken meat} & \multicolumn{4}{c}{Pork meat} \\
\hline
\hline
Cases & Controls & OR & 95\% CI & Cases & Controls & OR & 95\% CI & Cases & Controls & OR & 95\% CI \\
\hline
Never Exposed (Ref group) & 1,823 & 2,273 & 1.00 & --- & 1,823 & 2,273 & 1.00 & --- & 1,823 & 2,273 & 1.00 & --- \\
Ever Exposed & 117 & 108 & 1.22 & 0.90-1.67 & 136 & 129 & 1.19 & 0.91-1.55 & 145 & 143 & 1.09 & 0.83-1.42 \\
Duration of exposure & & & & & & & & & & & & \\
<5 years & 40 & 37 & 1.45 & 0.92-2.31 & 30 & 40 & 0.97 & 0.60-1.58 & 39 & 41 & 1.25 & 0.80-1.96 \\
6-15 years & 29 & 43 & 0.79 & 0.47-1.31 & 42 & 41 & 1.21 & 0.78-1.88 & 44 & 58 & 0.84 & 0.55-1.28 \\
>16 years & 48 & 28 & 1.63 & 0.95-2.88 & 64 & 48 & 1.36 & 0.90-2.06 & 61 & 43 & 1.28 & 0.81-2.03 \\
p-value of test for linear trend (with ref cat) & & & 0.23 & & & & 0.11 & & & & & 0.54 \\
Intensity of exposure & & & & & & & & & & & & \\
Low & 60 & 59 & 1.26 & 0.86-1.83 & 71 & 68 & 1.24 & 0.88-1.75 & 70 & 72 & 1.15 & 0.82-1.62 \\
Medium & 42 & 35 & 1.22 & 0.73-2.04 & 47 & 46 & 1.11 & 0.72-1.71 & 55 & 52 & 1.03 & 0.68-1.58 \\
High & 15 & 14 & 0.91 & 0.35-2.40 & 18 & 15 & 1.22 & 0.56-2.65 & 20 & 19 & 0.89 & 0.40-1.94 \\
p-value of test for linear trend (with ref cat) & & & 0.36 & & & & 0.29 & & & & & 0.78
\end{tabular}

```

```

\begin{tabular}{c}
\hline
\multicolumn{12}{c}{Table 1. Anticonvulsant activity and protective index of intraperitoneal AEDs in mice} \\
\hline
\multicolumn{12}{c}{Rotorod test & MES test & Phenytoin test & Bicuculline & Picrotoxin & Strychnine} \\
\hline
AED & TD_{50} (95\% CI) & PI & ED_{50} (95\% CI) & PI & ED_{50} (95\% CI) & PI & ED_{50} (95\% CI) & PI & ED_{50} (95\% CI) & PI & ED_{50} (95\% CI) & PI \\
Rofenol & 15.1 (12.5-18.1) & 23.2 & 54.0 (40.0-72.1) & 9.9 & 76.3 (60.0-96.0) & 9.9 & 76.3 (60.0-96.0) & 9.9 & 76.3 (60.0-96.0) & 9.9 & 76.3 (60.0-96.0) & 9.9 \\
Phenobarbital & 65.5 (52.2-72.1) & 4.9 & 13.2 (5.9-15.9) & 5.2 & 37.7 (26.5-47.4) & 1.8 & 27.5 (20.8-34.8) & 2.5 & 55.1 (40.8-72.1) & 0.7 & 95.3 (71.3-99.5) & 0.7 \\
Phenytoin & 69.0 (62.8-72.9) & 3.2 & 18.6 (12.2-25.7) & 2.9 & 45.9 (35.9-59.0) & 1.2 & 59.7 (31.1-144.0) & 1.1 & 29.2 (26.1-32.3) & 1.5 & 29.2 (26.1-32.3) & 1.5 \\
Valproate & 442.8 (381-460) & 1.4 & 12.3 (1.1-15.1) & 2.4 & 45.9 (35.9-59.0) & 1.2 & 59.7 (31.1-144.0) & 1.1 & 29.2 (26.1-32.3) & 1.5 & 29.2 (26.1-32.3) & 1.5 \\
Carbamazepine & 442.8 (381-460) & 1.4 & 12.3 (1.1-15.1) & 2.4 & 45.9 (35.9-59.0) & 1.2 & 59.7 (31.1-144.0) & 1.1 & 29.2 (26.1-32.3) & 1.5 & 29.2 (26.1-32.3) & 1.5 \\
\hline
\multicolumn{12}{c}{Maximum protection, 37.5\%} \\
\multicolumn{12}{c}{Maximum protection, 50.0\%} \\
\multicolumn{12}{c}{Maximum protection, 62.5\%} \\
\hline
\multicolumn{12}{c}{AED, antiepileptic drug; MES, maximal electroshock; TD_{50}, the dose eliciting evidence of minimal neurotoxicity in 50\% of animals; CI, confidence interval; ED_{50}, the dose of drug required to produce the desired end point in 50\% of animals; and PI, protective index (ratio of TD_{50} to ED_{50}).} \\
\hline
\end{tabular}

```

Figure 6. Showcase of Table-SE.

Visual Table

企业类型	目的	模式和特点	优势	典型企业
云服务提供商	以物联网为抓手带动上层应用服务业绩增长	目前多以提供底层计算资源、提供应用使能平台为主	在互联网领域中积累了丰富的技术、商业、生态经验 底层IaaS能力突出、共性技术能力提炼	阿里云、腾讯云、百度云、亚马逊AWS IoT等
通信领域厂商	获得流量业务收入、战略布局物联网、把握新增市场机遇	多以连接管理、应用使能平台为主要功能服务为主	在连接管理平台具有绝对优势、具有全球通用连接能力	电信运营商、通信设备厂商、中国移动ONENet、中国联通物联网平台、华为云IoT等
软件系统服务商	解决内部开发效率的问题、优化产品服务	以应用开发平台为主要服务内容为主	擅长软件设计、生产、管理、运维等服务、具备丰富的行业软件开发及服务经验	紫光云、广联达筑联等
垂直领域传统厂商	利用自身对行业的理解与经验、打造垂直平台、实现传统企业的转型升级	垂直专业领域的物联网平台	深刻的行业理解和行业技术、对行业有深度应用、拥有行业数据和客户资源	西门子、工业富联、美的M-Smart等企业
初创企业	看好物联网未来的发展潜力	目前阶段很多初创平台企业多以SaaS解决方案公司的形式存在	拥有与选定细分行业相关的软件、硬件经验、服务延伸到通用型平台厂商难以触及的细分领域、形成错位竞争	涂鸦智能、云智易、机智云、艾拉物联等

Site-B	Site-E	DEV	DD	Model
3-HCY	11-DGG	1.49	66.5	d-1
3-HCY	12-GGS	1.49	66.5	
4-CNY	1-GGH	1.29	74.8	
4-CNY	11-DGG	1.29	74.8	
4-CNY	12-GGS	1.29	74.8	d-2
5-YNT	1-GGH	1.39	70.3	
5-YNT	11-DGG	1.39	70.3	
5-YNT	12-GGS	1.39	70.3	
5-YNT	18-GGC	1.39	76.6	d-3
9-NND	1-GGH	1.85	69.2	
9-NND	12-GGS	1.85	69.2	
9-NND	18-GGC	1.85	73.9	

Ground Truth: LaTeX

```

\begin{tabular}{|l|l|l|l|l|} \hline
企业类型 & 目的 & 模式和特点 & 优势 & 典型企业 \\ \hline
云服务提供商 & 以物联网为抓手带动上层应用服务业绩增长 & 目前多以提供底层计算资源、提供应用使能平台为主 & 在互联网领域中积累了丰富的技术、商业、生态经验 & 阿里云、腾讯云、百度云、亚马逊AWS IoT等 \\ \hline
通信领域厂商 & 获得流量业务收入、战略布局物联网、把握新增市场机遇 & 多以连接管理、应用使能平台为主要功能服务为主 & 在连接管理平台具有绝对优势、具有全球通用连接能力 & 电信运营商、通信设备厂商、中国移动ONENet、中国联通物联网平台、华为云IoT等 \\ \hline
软件系统服务商 & 解决内部开发效率的问题、优化产品服务 & 以应用开发平台为主要服务内容为主 & 擅长软件设计、生产、管理、运维等服务、具备丰富的行业软件开发及服务经验 & 紫光云、广联达筑联等 \\ \hline
垂直领域传统厂商 & 利用自身对行业的理解与经验、打造垂直平台、实现传统企业的转型升级 & 垂直专业领域的物联网平台 & 深刻的行业理解和行业技术、对行业有深度应用、拥有行业数据和客户资源 & 西门子、工业富联、美的M-Smart等企业 \\ \hline
初创企业 & 看好物联网未来的发展潜力 & 目前阶段很多初创平台企业多以SaaS解决方案公司的形式存在 & 拥有与选定细分行业相关的软件、硬件经验、服务延伸到通用型平台厂商难以触及的细分领域、形成错位竞争 & 涂鸦智能、云智易、机智云、艾拉物联等 \\ \hline
\end{tabular}

```

```

\begin{tabular}{|l|l|l|l|l|} \hline
Site-B & Site-E & DEV & DD & Model \\ \hline
3-HCY & 11-DGG & 1.49 & 66.5 & \\ \hline
3-HCY & 12-GGS & 1.49 & 66.5 & \\ \hline
4-CNY & 1-GGH & 1.29 & 74.8 & d-1 \\ \hline
4-CNY & 11-DGG & 1.29 & 74.8 & \\ \hline
4-CNY & 12-GGS & 1.29 & 74.8 & \\ \hline
5-YNT & 1-GGH & 1.39 & 70.3 & d-2 \\ \hline
5-YNT & 11-DGG & 1.39 & 70.3 & \\ \hline
5-YNT & 12-GGS & 1.39 & 70.3 & \\ \hline
5-YNT & 18-GGC & 1.39 & 76.6 & \\ \hline
9-NND & 1-GGH & 1.85 & 69.2 & d-3 \\ \hline
9-NND & 12-GGS & 1.85 & 69.2 & \\ \hline
9-NND & 18-GGC & 1.85 & 73.9 & \\ \hline
\end{tabular}

```

Figure 7. Showcase of Table-SE.

thumbnail images as input for  $E^g$  without employing the widely-used Dynamic High Resolution (DHR) technique [12, 30]. In the Visual Instruction Tuning stage, DHR is introduced, allowing up to six times more visual tokens. At this stage, we apply the Generalist-Specialist Collaboration Masking (GSCM) mechanism with a masking ratio of 0.3 to constrain  $E^g$ , encouraging the model to leverage domain-specific information from expert models. For train-

able modules, the Domain-General Knowledge Alignment stage updates only the General Projector  $P^g$  and Expert Projector Set  $S^e$ . In subsequent stages, the General Projector  $P^g$ , Expert Projector Set  $S^e$ , and Language Model  $f$  are updated.

		Domain-General Knowledge Alignment	Visual Instruction Tuning	
Vision	Resolution	General Encoder $E^g$	448	$448 \times \{ \{1,2,3,4,5,6\} \times 1, 1 \times \{2,3,4,5,6\}, 2 \times \{2,3\}, 3 \times 2 \}$
		Table Encoder $E^{table}$	N/A	N/A
		Chart Encoder $E^{chart}$	N/A	N/A
		Math Encoder $E^{math}$	336	336
	#Tokens	General Encoder $E^g$	256	Max $256 \times 6$
		Table Encoder $E^{table}$	2048	2048
		Chart Encoder $E^{chart}$	2048	2048
		Math Encoder $E^{math}$	576	576
	Total Tokens		$256 + \{0, 2048, 2048, 576\}$	Max $256 \times 6 + \{0, 2048, 2048, 576\}$
	Training	#Samples	1.1M	2.6M
GSCM ratio		N/A	0.3	
Dynamic High Res [12]		False	True	
Trainable		General Projector $P^g$ , Expert Projector Set $S^e$	General Projector $P^g$ , Expert Projector Set $S^e$ , Language Model $f$	
Batch Size		256/128	128	
LR		4e-5/2e-5	2e-5/1e-5	
Warm Up		100 steps	0.03 ratio	
LR Scheduler		Consine	Consine	
Max Length		4096	8192	
Weight Decay		0.01	0.01	
Epoch		1	1	

Table 15. Detailed configuration for each training stage of Chimera in multi-modal reasoning scenario. The table outlines the progression of vision parameters, dataset characteristics and training hyperparameters. For elements containing “/”, the left side represents configurations used by the 2B and 4B model, while the right side represents configurations used by the 8B model.

		Domain-General Knowledge Alignment	Visual Instruction Tuning	
Vision	Resolution	General Encoder $E^g$	448	$448 \times \{ \{1,2,3,4,5,6\} \times 1, 1 \times \{2,3,4,5,6\}, 2 \times \{2,3\}, 3 \times 2 \} \}$
		Document Encoder $E^{document}$	1024	1024
	#Tokens	General Encoder $E^g$	256	Max 256×6
		Document Encoder $E^{document}$	256	256
	Total Tokens		256 + 256	Max 256×6 + 256
Training	#Samples	995K	275K	
	GSCM ratio	N/A	0.3	
	Dynamic High Res [12]	False	True	
	Trainable	General Projector $P^g$ , Expert Projector Set $S^e$	General Projector $P^g$ , Expert Projector Set $S^e$ , Language Model $f$	
	Batch Size	256	128	
	LR	4e-5	2e-5	
	Warm Up	100 steps	0.03 ratio	
	LR Scheduler	Consine	Consine	
	Max Length	4096	8192	
	Weight Decay	0.01	0.01	
	Epoch	1	1	

Table 16. Detailed configuration for each training stage of Chimera in visual content extraction scenario. The table outlines the progression of vision parameters, dataset characteristics and training hyperparameters.

## 15. Visualization of Chimera on Visual Content Extraction

### 15.1. Table Format Transformation

We provide the rendered table of the output results of Chimera-8B to show its table format transformation performance. As shown in Fig. 8, Fig. 9 and Fig. 10, Chimera excels in extracting and formatting table content from both Arxiv-style and more diverse table layouts with high accuracy.

### 15.2. Chart Structural Extraction

We provide the rendered table of the output results of Chimera-8B to show its chart structural extraction performance. As shown in Fig. 11, Fig. 12 and Fig. ??, Chimera can identify and extract information from various types of charts, such as pie charts, line graphs, bar charts, etc., and output this information in a structured format accurately.

# Input: Visual Table

资产负债表					
	2020	2021	2022E	2023E	2024E
货币资金	703.3	604.1	2,111.4	2,582.9	2,817.4
交易性金融资产	-	-	-	-	-
应收账款	1,066.7	1,307.4	1,507.8	1,720.8	2,801.0
应收票据	85.6	163.1	72.2	157.3	147.1
预付账款	56.4	54.9	89.0	86.7	116.8
存货	779.0	648.3	1,009.8	1,053.6	1,519.6
其他流动资产	670.3	448.3	414.6	511.1	274.8
可供出售金融资产	-	-	-	-	-
持有至到期投资	-	-	-	-	-
长期股权投资	60.7	36.9	36.9	36.9	36.9
投资性房地产	5.0	13.2	13.2	13.2	13.2
固定资产	445.5	502.8	459.0	415.2	371.5
在建工程	24.4	29.0	29.0	29.0	29.0
无形资产	107.8	98.8	86.7	74.6	62.5
其他非流动资产	1,274.9	1,705.5	1,498.7	1,490.2	1,290.6
资产总额	5,279.6	5,612.2	7,328.3	8,171.5	9,480.2
短期债务	736.6	809.5	1,460.2	2,054.8	1,482.0
应付账款	1,554.8	1,651.2	2,027.4	1,942.5	2,822.0
应付票据	109.3	124.5	23.3	153.6	60.8
其他流动负债	516.5	613.7	581.4	580.4	584.1
长期借款	240.4	60.1	422.8	189.0	-
其他非流动负债	53.4	111.7	65.8	76.9	84.8
负债总额	3,210.9	3,370.6	4,580.8	4,997.2	5,033.8
少数股东权益	208.0	111.5	118.1	129.1	142.4
股本	774.8	772.8	772.8	772.8	772.8
留存收益	1,290.0	1,662.1	2,059.7	2,557.2	3,134.9
股东权益	2,068.6	2,241.6	2,747.6	3,174.3	4,446.4

主要财务指标	2021A	2022E	2023E	2024E
营业收入	19515	23852	27760	31884
收入同比 (%)	45.1%	22.2%	16.4%	14.9%
归属母公司净利润	1150	1339	1671	2002
净利润同比 (%)	43.9%	16.4%	24.8%	19.8%
毛利率 (%)	12.6%	12.7%	13.6%	13.9%
ROE (%)	15.8%	15.9%	17.0%	17.4%
每股收益 (元)	2.19	2.52	3.15	3.77
P/E	24.45	14.59	11.69	9.76
P/B	3.91	2.33	1.99	1.70
EV/EBITDA	15.29	6.19	4.85	3.80

	RPCB多层板	软板+模组	HDI	IC载板
2022(E)	387.21	138.42	117.63	174.15
2023(F)	373.40	134.27	115.28	160.73
2024(F)	381.79	141.31	122.25	174.41
2025(F)	419.39	148.72	129.65	189.26
2026(F)	444.30	156.52	137.49	205.38
2027(F)	450.48	164.73	145.81	222.86
2022-2027 CAGR	3.1%	3.5%	4.4%	5.1%

# Output: LaTeX

资产负债表					
	2020	2021	2022E	2023E	2024E
货币资金	703.3	604.1	2,111.4	2,582.9	2,817.4
交易性金融资产	-	-	-	-	-
应收账款	1,066.7	1,307.4	1,507.8	1,720.8	2,801.0
应收票据	85.6	163.1	72.2	157.3	147.1
预付账款	56.4	54.9	89.0	86.7	116.8
存货	779.0	648.3	1,009.8	1,053.6	1,519.6
其他流动资产	670.3	448.3	414.6	511.1	274.8
可供出售金融资产	-	-	-	-	-
持有至到期投资	-	-	-	-	-
长期股权投资	60.7	36.9	36.9	36.9	36.9
投资性房地产	5.0	13.2	13.2	13.2	13.2
固定资产	445.5	502.8	459.0	415.2	371.5
在建工程	24.4	29.0	29.0	29.0	29.0
无形资产	107.8	98.8	86.7	74.6	62.5
其他非流动资产	1,274.9	1,705.5	1,498.7	1,490.2	1,290.6
资产总额	5,279.6	5,612.2	7,328.3	8,171.5	9,480.2
短期负债	736.6	809.5	1,460.2	2,054.8	1,482.0
应付账款	1,554.8	1,651.2	2,027.4	1,942.5	2,822.0
应付票据	109.3	124.5	23.3	153.6	60.8
其他流动负债	516.5	613.7	581.4	580.4	584.1
长期借款	240.4	60.1	422.8	189.0	-
其他非流动负债	53.4	111.7	65.8	76.9	84.8
负债总额	3,210.9	3,370.6	4,580.8	4,997.2	5,033.8
少数股东权益	208.0	111.5	118.1	129.1	142.4
股本	774.8	772.8	772.8	772.8	772.8
留存收益	1,290.0	1,662.1	2,059.7	2,557.2	3,134.9
股东权益	2,068.6	2,241.6	2,747.6	3,174.3	4,446.4

主要财务指标	2021A	2022E	2023E	2024E
营业收入	19515	23852	27760	31884
收入同比增长 (%)	45.1%	22.2%	16.4%	14.9%
归属于母公司净利润	1150	1339	1671	2002
净利润同比增长 (%)	43.9%	16.4%	24.8%	19.8%
毛利率 (%)	12.6%	12.7%	13.6%	13.9%
ROE (%)	15.8%	15.9%	17.0%	17.4%
每股收益 (元)	2.19	2.52	3.15	3.77
P/E	24.45	14.59	11.69	9.76
P/B	3.91	2.33	1.99	1.70
EV/EBITDA	15.29	6.19	4.85	3.80

	RPCB 多层板	软板 + 模组	HDI	IC 载板
2022(E)	387.21	138.42	117.63	174.15
2023(F)	373.40	134.27	115.28	160.73
2024(F)	381.79	141.31	122.25	174.41
2025(F)	419.39	148.72	129.65	189.26
2026(F)	444.30	156.52	137.49	205.38
2027(F)	450.48	164.73	145.81	222.86
2022-2027 CAGR	3.1%	3.5%	4.4%	5.1%

Figure 8. Output of Chimera-8B on Table Format Transformation.

## 15.3. Document Context Extraction

We provide the rendered page of the output results of Chimera to show its document content extraction performance. As shown in Fig. 14, Fig. 15, Fig. 16 and Fig. 17, Chimera demonstrates exceptional content extraction ca-

pabilities on both single-column and double-column documents, effectively extracting structured information end-to-end from text-dense visual inputs.



# Input: Visual Table

Star	Sp. type	P <sub>rot</sub> (days)	P <sub>cyc</sub> (range) (years)	lit <sup>c</sup>	P <sub>cyc</sub> , Balinuas et al. (years)
simple cycles					
HD 3651	K0V <sup>a</sup>	44 <sup>b</sup>	11.6(9.57–13.7)-lt	yes	13.8±0.4
HD 4628	K2.5V <sup>a</sup>	41.6	8.94(8.30–9.5)	no	8.37±0.08
HD 10476	K1V <sup>a</sup>	33.7	9.8(9.01–9.85)	no	9.6±0.1
HD 16160	K3V <sup>a</sup>	57	12.1	no	13.2±0.2
HD 26965	K1V <sup>a</sup>	43 <sup>b</sup>	10.0(9.57–10.5)	no	10.1±0.1
HD 32147	K3+V <sup>a</sup>	39.3	10.6(9.85–11.3), lt	yes	11.1±0.2
HD 81809	G5V <sup>a</sup>	39.3	8.69(8.10–9.28)	no	8.17±0.08
HD 103995	K1V <sup>a</sup>	36.5	6.95(6.9–7.0), lt	yes	7.30±0.08
HD 160346	K2.5V <sup>a</sup>	35.3	7.35(7.2–7.5), lt	yes	7.00±0.08
HD 166620	K2V <sup>c</sup>	41.5	13.6(9.6–17.6)	no	15.8±0.3
HD 201091	K5V	37.1	6.95(6.7–7.2), lt	yes	7.3±0.1
HD 219834B	K2V	34.0	9.29(9.01–9.57)	no	10.0±0.2
Sun	G2V	27.275	11(9–14), 3.65(3.3–4.0) <sup>d</sup>	yes	
complicated cycles					
HD 1835	G2V <sup>a</sup>	7.84	7.6(7.3–7.9), 2.4(2.50–2.28), 3.97(4.85–3.09), lt	yes	9.1±0.3
HD 20630	G5V	9.08	5.32(5.36–5.27)	no	5.6±0.1
HD 76151	G3V <sup>a</sup>	15.2	5.32(6.07–4.56), lt	yes	2.52±0.02
HD 78366	G0V	9.7	13.45(12.6–14.3)-lt, 4.0(3.85–4.15)	yes	12.2±0.4, 5.9±0.1
HD 95735	M2V	54	3.90(3.75–4.04), 12.7(10.3–15.0)-lt	yes	
HD 100180	F9.5V <sup>a</sup>	14.6	13.2(16.6–9.85), 3.63	no	3.56±0.04, 12.9±0.5
HD 114710	G0V	12.9	16.6(17.6–13.7–18.6), 7.7(7.2–8.2), 5.25(5.1–5.4)	no	16.6±0.6, 9.6±0.3
HD 115404	K2.5V <sup>a</sup>	18.8	10.8(9.57–12.1), 5.08(5.83–4.33), 3.4(3.96–2.84) lt	yes	12.4±0.4
HD 131156A	G8V	6.25	3.7(3.6–3.8), 12, lt	yes	
HD 131156B	K4V	11.05	4.2(4.64–3.76), 2.28, lt	yes	
HD 149661	K0V <sup>a</sup>	21.3	4.0, 6.2(5.6–6.8), 12.25(11.3–13.2)-lt	yes	17.4±0.7, 4.00±0.04
HD 152391	G8+V <sup>a</sup>	11.4	9.9(12.6–7.17), 2.8(2.5–3.1)	no	10.9±0.2
HD 156026	K5V	29.2	4.33(3.95–4.71), 8.1, lt(≈20)	yes	21.0±0.9
HD 165341A	K0V <sup>a</sup>	18.9	11.4(9–13.8), 5.17, lt	yes	5.1±0.1
HD 165341B	K6V	–	Var	yes	Var
HD 190406	G0V <sup>a</sup>	15.5	15.8(15.0–17.6)-lt, 8.35(7.69–9.01), 4.65(4.44–4.86), 2.33, 3.01	yes	2.60±0.02, 16.9±0.8
HD 201092	K7V	34.1	13.4(10.1–16.6)-lt, 4.45(4.71–4.18), (2.07:)	yes	11.7±0.4

# Output: LaTeX

Star	Sp. type	P <sub>rot</sub> (days)	P <sub>cyc</sub> (range) (years)		lit <sup>c</sup>	P <sub>cyc</sub> , Balinuas et al. (years)					
simple cycles											
HD 3651	K0V <sup>a</sup>	44 <sup>b</sup>	11.6(9.57–13.7)-lt		yes	13.8±0.4					
HD 4628	K2.5V <sup>a</sup>	41.6	8.94(8.30–9.5)		no	8.37±0.08					
HD 10476	K1V <sup>a</sup>	33.7	9.8(9.01–9.85)		no	9.6±0.1					
HD 16160	K3V <sup>a</sup>	57	12.1		no	13.2±0.2					
HD 26965	K1V <sup>a</sup>	43 <sup>b</sup>	10.0(9.57–10.5)		no	10.1±0.1					
HD 32147	K3+V <sup>a</sup>	39.3	10.6(9.85–11.3), lt		yes	11.1±0.2					
HD 81809	G5V <sup>a</sup>	39.3	8.69(8.10–9.28)		no	8.17±0.08					
HD 103995	K1V <sup>a</sup>	36.5	6.95(6.9–7.0), lt		yes	7.30±0.08					
HD 160346	K2.5V <sup>a</sup>	35.3	7.35(7.2–7.5), lt		yes	7.00±0.08					
HD 166620	K2V <sup>c</sup>	41.5	13.6(9.6–17.6)		no	15.8±0.3					
HD 201091	K5V	37.1	6.95(6.7–7.2), lt		yes	7.3±0.1					
HD 219834B	K2V	34.0	9.29(9.01–9.57)		no	10.0±0.2					
Sum	G2V	27.275	11(9–14), 3.65(3.3–4.0) <sup>d</sup>		yes						
complicated cycles											
HD 1835	G2V <sup>a</sup>	7.84	7.6(7.3–7.9), 2.4(2.50–2.28), 3.97(4.85–3.09), lt		yes	9.1±0.3					
HD 20630	G5V	9.08	5.32(5.36–5.27)		no	5.6±0.1					
HD 76151	G3V <sup>a</sup>	15.2	5.32(6.07–4.56), lt		yes	2.52±0.02					
HD 78366	G0V	9.7	13.45(12.6–14.3)-lt, 4.0(3.85–4.15)		yes	12.2±0.4, 5.9±0.1					
HD 95735	M2V	54	3.90(3.75–4.04), 12.7(10.3–15.0)-lt		yes						
HD 100180	F9.5V <sup>a</sup>	14.6	13.2(16.6–9.85), 3.63		no	3.56±0.04, 12.9±0.5					
HD 114710	G0V	12.9	16.6(17.6–13.7–18.6), 7.7(7.2–8.2), 5.25(5.1–5.4)		no	16.6±0.6, 9.6±0.3					
HD 115404	K2.5V <sup>a</sup>	18.8	10.8(9.57–12.1), 5.08(5.83–4.33), 3.4(3.96–2.84) lt		yes	12.4±0.4					
HD 131156A	G8V	6.25	3.7(3.6–3.8), 12, lt		yes						
HD 131156B	K4V	11.05	4.2(4.64–3.76), 2.28, lt		yes						
HD 149661	K0V <sup>a</sup>	21.3	4.0, 6.2(5.6–6.8), 12.25(11.3–13.2)-lt		yes	17.4±0.7, 4.00±0.04					
HD 152391	G8+V <sup>a</sup>	11.4	9.9(12.6–7.17), 2.8(2.5–3.1)		no	10.9±0.2					
HD 156026	K5V	29.2	4.33(3.95–4.71), 8.1, lt(approximately 20)		yes	21.0±0.9					
HD 165341A	K0V <sup>a</sup>	18.9	11.4(9–13.8), 5.17, lt		yes	5.1±0.1					
HD 165341B	K6V	—	—		yes	Var					
HD 190406	G0V <sup>a</sup>	15.5	15.8(15.0–17.6)-lt, 8.35(7.69–9.01), 4.65(4.44–4.86), 2.33, 3.01		yes	2.60±0.02, 16.9±0.8					
HD 201092	K7V	34.1	13.4(10.1–16.6)-lt, 4.45(4.71–4.18), (2.07:)		yes	11.7±0.4					
Controls											
		Hodgkin lymphoma		Non-Hodgkin lymphoma							
		Cases	OR	95% CI	Cases	OR	95% CI				
Never Exposed (reference group)	2,273	315	1.00	–	1,823	1.00	–				
Ever Exposed	189	24	1.06	0.65–1.71	184	1.18	0.95–1.46				
Duration of exposure											
<5 years	52	12	1.14	0.57–2.30	49	1.25	0.84–1.86				
6–15 years	62	8	0.98	0.44–2.20	52	1.04	0.71–1.51				
≥16 years	73	4	1.02	0.36–2.90	82	1.27	0.92–1.76				
p-value of test for linear trend				0.90			0.13				
Weighted duration of exposure											
<6 months	62	14	1.54	0.79–2.99	57	1.10	0.76–1.59				
7 months to 1 year	35	3	0.60	0.17–2.13	40	1.39	0.87–2.20				
>1 year	90	7	0.84	0.37–1.91	86	1.17	0.87–1.59				
p-value of test for linear trend				0.75			0.13				
Intensity of exposure											
Low	84	11	1.05	0.52–2.12	85	1.24	0.91–1.70				
Medium	70	10	1.19	0.56–2.49	66	1.11	0.79–1.57				
High	35	3	0.80	0.23–2.74	32	1.14	0.70–1.85				
50 days											
100 days											
		F*	P	G	S	B	F	P	G	S	B
Collembola total		20.7	10.4	5.98	18.2	45.3	17.2	10.8	9.4	16.4	68.8
Isotoma notabilis		3.56	3.06	2.51	3.85	29.5	4.02	5.94	6.85	5.95	47.3
Mesaphorura yosii		0	1.79	1.04	1.72	3.29	7.56	1.43	0.96	1.95	2.53
Micraphorura absoloni		0	0.19	0.36	0.18	1.24	2.25	0.92	0.06	2.46	7.13
Willemia anophthalmia		0	3.61	1.0	8.1	4.37	1.63	1.54	0.88	0.06	3.29
Anurida pygmaea		0	0.09	0.04	0.55	0.97	0.59	0.48	0.15	0.09	2.1
Frieseca mirabilis		0	0.24	0.04	0.22	0	0.3	0.4	0.15	0.82	0.14
Pseudanurophorus binoculatus		0	0.42	0.23	0.13	1.18	0.26	0	0	0	0.72
Isotomiella minor		0	0	0.21	1.28	0.31	0.15	0	0.32	4.82	4.52

Figure 9. Output of Chimera-8B on Table Format Transformation.

Input: Visual Table

会计年度	2021A	2022A	2023E	2024E	2025E
营业收入(百万元)	11,339	11,008	15,123	16,828	18,396
YoY(%)	14.6	-2.9	37.4	11.3	9.3
净利润(百万元)	101	113	1,392	1,991	2,200
YoY(%)	-8.7	12.8	1126.8	43.0	10.5
毛利率(%)	34.2	33.1	41.1	47.6	47.7
EPS(摊薄/元)	0.09	0.11	1.30	1.86	2.06
ROE(%)	1.7	1.4	8.7	11.2	11.1
P/E(倍)	408.4	362.1	29.5	20.6	18.7
P/B(倍)	2.5	2.5	2.3	2.1	1.9
净利率(%)	0.9	1.0	9.2	11.8	12.0

8月排名	证券简称	占比(%)	7月排名	证券简称	占比(%)
1	中天科技	8.37%	1	中天科技	8.43%
2	中际旭创	5.07%	2	中际旭创	4.43%
3	新易盛	4.59%	3	烽火通信	4.36%
4	普天科技	4.02%	4	中国联通	4.24%
5	中国移动	3.84%	5	新易盛	4.15%
6	中国联通	3.68%	6	中兴通讯	3.82%
7	华测导航	3.58%	7	华测导航	3.60%
8	中兴通讯	3.50%	8	天孚通信	3.52%
9	亿联网络	3.03%	9	普天科技	3.41%
10	烽火通信	2.87%	10	中国移动	3.32%

公司名称	2023年11月累计保费收入 (亿元)	同比增速	当月保费收入 (亿元)	环比增速
人保财险	4727	6.8%	329	8.8%
车险	2543	5.5%	247	7.7%
非车险	2184	8.3%	82	12.1%
平安财险	2736	1.4%	243	3.4%
太保财险	1748	11.8%	138	9.7%
合计	9211	6.0%	709	7.0%

Output: LaTeX

会计年度	2021A	2022A	2023E	2024E	2025E
营业收入(百万元)	11,339	11,008	15,123	16,828	18,396
YoY(%)	14.6	-2.9	37.4	11.3	9.3
净利润(百万元)	101	113	1,392	1,991	2,200
YoY(%)	-8.7	12.8	1126.8	43.0	10.5
毛利率(%)	34.2	33.1	41.1	47.6	47.7
EPS(摊薄/元)	0.09	0.11	1.30	1.86	2.06
ROE(%)	1.7	1.4	8.7	11.2	11.1
P/E(倍)	408.4	362.1	29.5	20.6	18.7
P/B(倍)	2.5	2.5	2.3	2.1	1.9
净利率(%)	0.9	1.0	9.2	11.8	12.0

8月排名	证券简称	占比(%)	7月排名	证券简称	占比(%)
1	中天科技	8.37%	1	中天科技	8.43%
2	中际旭创	5.07%	2	中际旭创	4.43%
3	新易盛	4.59%	3	烽火通信	4.36%
4	普天科技	4.02%	4	中国联通	4.24%
5	中国移动	3.84%	5	新易盛	4.15%
6	中国联通	3.68%	6	中兴通讯	3.82%
7	华测导航	3.58%	7	华测导航	3.60%
8	中兴通讯	3.50%	8	天孚通信	3.52%
9	亿联网络	3.03%	9	普天科技	3.41%
10	烽火通信	2.87%	10	中国移动	3.32%

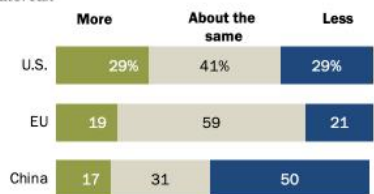
公司名称	2023年11月累计保费收入	同比增长	当月保费收入	环比增速
人保财险	4727	6.8%	329	8.8%
车险	2543	5.5%	247	7.7%
非车险	2184	8.3%	82	12.1%
平安财险	2736	1.4%	243	3.4%
太保财险	1748	11.8%	138	9.7%
合计	9211	6.0%	709	7.0%

Figure 10. Output of Chimera-8B on Table Format Transformation.

## Input: Visual Chart

### Many think China's global influence will decline after the coronavirus outbreak

% who say each will have \_\_\_ influence in world affairs after the coronavirus outbreak compared to before the outbreak



Note: No answer responses not shown.

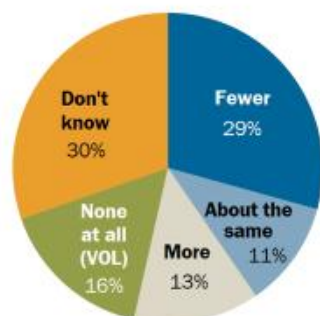
Source: Survey of U.S. adults conducted April 29-May 5, 2020.

\*Americans Give Higher Ratings to South Korea and Germany Than U.S. for Dealing With Coronavirus

PEW RESEARCH CENTER

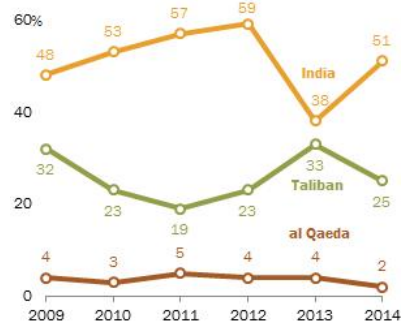
### Little appetite for allowing more immigrants into India

India should allow \_\_\_ immigrants



### Concerns about India on the Rise Again

Which is the greatest threat to Pakistan?



Source: Spring 2014 Global Attitudes survey. Q117.

PEW RESEARCH CENTER

## Output: Markdown

Entity	More	About the same	Less
China	17	31	50
EU	19	59	21
U.S.	29	41	29

Entity	Value
About the same	11
More	13
None at all (VOL)	16
Don't know	30
Fewer	29

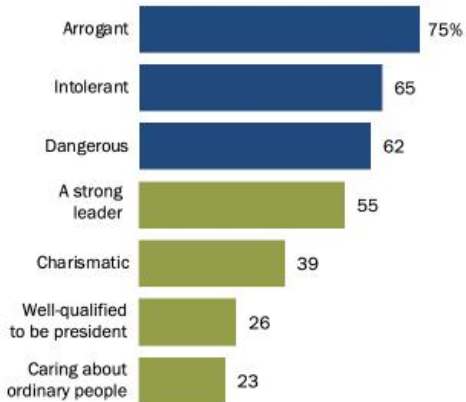
Entity	2009	2010	2011	2012	2013	2014
al Qaeda	4.0	3.0	5.0	4.0	4.0	2.0
Taliban	32.0	23.0	19.0	23.0	33.0	25.0
India	48.0	53.0	57.0	59.0	38.0	51.0

Figure 11. Output of Chimera-8B on Chart Structural Extraction.

## Input: Visual Chart

### Global views of Trump's characteristics

% who say they think of President Donald Trump as ...

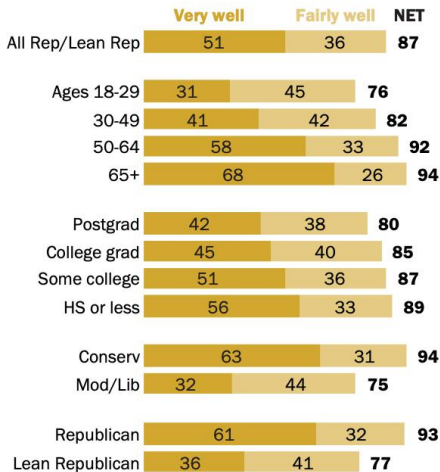


Note: Percentages are global medians based on 37 countries.  
Source: Spring 2017 Global Attitudes Survey.

PEW RESEARCH CENTER

### Older Republicans especially likely to see Trump as fighting for their beliefs

Among **Republicans and Republican leaners**, % who say the phrase 'fights for what I believe in' describes Trump ...



Note: Based on Republicans and Republican-leaning independents.  
Source: Survey of U.S. adults conducted Feb. 4-15, 2020.

PEW RESEARCH CENTER

## Output: Markdown

Entity	Value
Caring about ordinary people	23
Well-qualified to be president	26
Charismatic	39
A strong leader	55
Dangerous	62
Intolerant	65
Arrogant	75

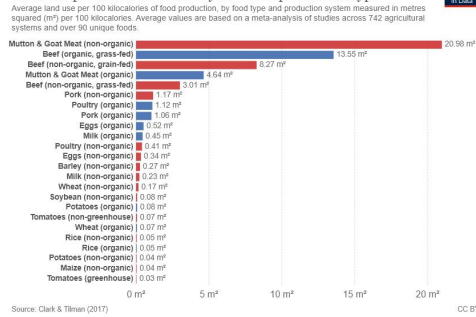
Entity	Very well	Fairly well	NET
Lean Republican	36	41	77
Republican	61	32	93
Mod/Lib	32	44	75
Conserv	63	31	94
HS or less	56	33	89
Some college	51	36	87
College grad	45	40	85
Postgrad	42	38	80
65+	68	26	94
50-64	58	33	92
30-49	41	42	82
Ages 18-29	31	45	76
All Rep/Lean Rep	51	36	87

Figure 12. Output of Chimera-8B on Chart Structural Extraction.

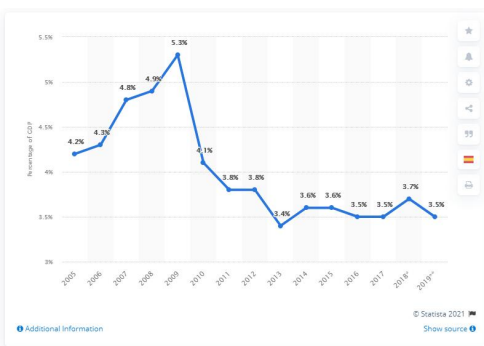
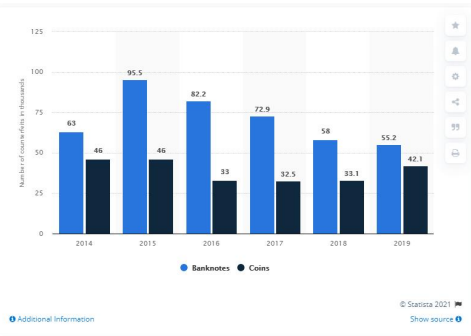
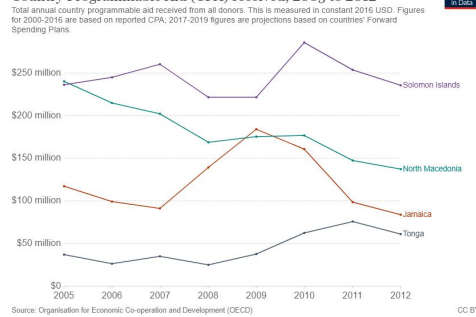


## Input: Visual Chart

### Land use per 100 kilocalories by food and production type



### Country Programmable Aid (CPA) received, 2005 to 2012



## Output: Markdown

Country	Land use per 100 kilocalories by food and production type
Mutton & Goat Meat (non-organic)	20.98 m²
Beef (organic, grass-fed)	13.55 m²
Beef (non-organic, grain-fed)	8.27 m²
Mutton & Goat Meat (organic)	4.64 m²
Beef (non-organic, grass-fed)	3.01 m²
Pork (non-organic)	1.17 m²
Poultry (organic)	1.12 m²
Pork (organic)	1.06 m²
Eggs (organic)	0.52 m²
Milk (organic)	0.45 m²
Poultry (non-organic)	0.41 m²
Eggs (non-organic)	0.34 m²
Barley (non-organic)	0.27 m²
Milk (non-organic)	0.23 m²
Wheat (non-organic)	0.17 m²
Soybean (non-organic)	0.08 m²
Potatoes (organic)	0.08 m²
Tomatoes (non-greenhouse)	0.07 m²
Wheat (organic)	0.07 m²
Rice (non-organic)	0.05 m²
Rice (organic)	0.05 m²
Potatoes (non-organic)	0.04 m²
Maize (non-organic)	0.04 m²
Tomatoes (greenhouse)	0.03 m²

Entity	2005	2006	2007	2008	2009	2010	2011	2012
Solomon Islands	239.0	246.0	265.0	223.0	223.0	286.0	256.0	237.0
North Macedonia	239.0	214.0	202.0	171.0	179.0	179.0	148.0	138.0
Jamaica	119.0	99.0	93.0	141.0	186.0	163.0	99.0	86.0
Tonga	38.0	28.0	38.0	26.0	37.0	63.0	77.0	62.0

Characteristic	Banknotes	Coins
2019	55.2	42.1
2018	58.0	33.1
2017	72.9	32.5
2016	82.2	33.0
2015	95.5	46.0
2014	63.0	46.0

Characteristic	Percentage of GDP
2019**	3.5%
2018*	3.7%
2017	3.5%
2016	3.5%
2015	3.6%
2014	3.6%
2013	3.4%
2012	3.8%
2011	3.8%
2010	4.1%
2009	5.3%
2008	4.9%
2007	4.8%
2006	4.3%
2005	4.2%

Figure 13. Output of Chimera-8B on Chart Structural Extraction.

# Input: Document Page

HYDROLOGICAL PROCESSES  
*Hydrol. Process.* **16**, 3131–3150 (2002)  
Published online 7 August 2002 in Wiley InterScience (www.interscience.wiley.com). DOI: 10.1002/hyp.1092

## Daily streamflow modelling and assessment based on the curve-number technique

Jin-Yong Choi,<sup>1</sup>\* Bernard A. Engel<sup>1</sup> and Ha Woo Chung<sup>2</sup>

<sup>1</sup> Department of Agricultural and Biological Engineering, Purdue University, West Lafayette, IN 47907-1146, USA.

<sup>2</sup> Division of Biological Resources and Material Engineering, Seoul National University, Suwon, Kyonggi 441-744, South Korea

### Abstract:

A cell-based long-term hydrological model (CELTHYM) that can be integrated with a geographical information system (GIS) was developed to predict continuous stream flow from small agricultural watersheds. The CELTHYM uses a cell-by-cell soil moisture balance approach. For surface runoff estimation, the curve number technique considering soil moisture on a daily basis was used, and release rate was used to estimate baseflow. Evapotranspiration was computed using the FAO modified Penman equation that considered land-use-based crop coefficients, soil moisture and the influence of topography on radiation. A rice paddy field water budget model was also adapted for the specific application of the model to East Asia. Model sensitivity analysis was conducted to obtain operational information about the model calibration parameters. The CELTHYM was calibrated and verified with measured runoff data from the WS#1 and WS#3 watersheds of the Seoul National University, Department of Agricultural Engineering, in Hwasong County, Kyonggi Province, South Korea. The WS#1 watershed is comprised of about 35.4% rice paddy fields and 42.3% forest, whereas the WS#3 watershed is about 85.0% forest and 11.5% rice paddy fields. The CELTHYM was calibrated for the parameter release rate,  $K$ , and soil moisture storage coefficient,  $STC$ , and results were compared with the measured runoff data for 1986. The validation results for WS#1 considering all daily stream flow were poor with  $R^2$ ,  $E^2$  and RMSE having values of 0.40, -6.63 and 9.69 (mm), respectively, but validation results for days without rainfall were statistically significant ( $E^2 = 0.66$ ). Results for WS#3 showed good agreement with observed data for all days, and  $R^2$ ,  $E^2$  and RMSE were 0.92, 0.91 and 2.23 (mm), respectively, suggesting potential for CELTHYM application to other watersheds. The direct runoff and water balance components for watershed WS#1 with significant areas of paddy fields did not perform well, suggesting that additional study of these components is needed. Copyright © 2002 John Wiley & Sons, Ltd.

**KEY WORDS** watershed modelling; GIS; soil moisture balance; grid-based modelling; paddy field water balance; model calibration; sensitivity analysis; model assessment

### INTRODUCTION

Water resources development and watershed management require an understanding of hydrological variations owing to changes in watershed characteristics over long-term periods (Bhaduri *et al.*, 2000), and spatial variability of watershed characteristics that affect hydrological phenomenon also must be evaluated in heterogeneous land-use watersheds. However, hydrological model operations that reflect long-term watershed changes often have limitations owing to difficulties obtaining measured hydrological data and data quantifying land use and soil characteristics. Therefore, simulation of stream flow on a daily basis using a long-term hydrological model that is simple to operate with readily available data is needed.

Continuous models, also called long-term hydrological models or continuous stream flow models, typically are focused on estimating water yield from a watershed. Owing to complications and difficulties related to data preparation and operation, however, these hydrological models largely have been used for daily, 10-day and

11 | One View, London Borough of Barking and Dagenham, London, UK

Gaining staff support is also key to ensuring the tool's continued improvement. Addressing the challenge of data linkage specifically, Katy Brown said: "We are doing more to communicate to users why, in some instances, they might not be able to view a record or why it is matched incorrectly (i.e., conflicting information in different case management systems), which is not the fault of One View directly. At a high level, this is to try and lift staff understanding of the process and to maintain trust/understanding in the system."

- **Clear feedback mechanism:** It is important to the project team that improvements to One View are driven by frontline staff feedback. Jill Gallagher described how this works in practice: "Frontline staff give us some great narratives around what's going on for them and how the needs have changed for the people they're serving. We are able to take that information and then adapt One View to meet that need." This may involve going back to the individual services to address data quality issues: "We have in some areas gone back to services to address some data quality issues and improve things from the point of data entry," said Rhodri Rowlands. This was echoed by Katy Brown: "If staff find information in a case summary they know to be wrong, then we are doing a big push for staff to report it, so we can look at it in the background and amend."

For example, staff feedback has led to increased frequency of data collection. As described in the Key challenges section, data is extracted at different frequencies and can be out of date. Debt information used to be extracted monthly, but LBBd have increased the frequency of these extracts to weekly based on staff feedback. "We are speaking to staff to identify the priority datasets and do what we can to increase their frequency and mitigate the impact of 'time' on the data presented," said Katy Brown.

- **Information governance (IG):** for the service delivery team, it's been very reassuring to know that there is robust IG. Gill Wilson describes her confidence in the tool's IG compliance: "One View has got a very, very good structure to it that embeds the Data Protection Act, the EU's General Data Protection Regulation, so that you know whenever you go in, you only get access to what is at your level. The formal process around the data protection, but also the formal process around the governance structure with the board and everything, it all feeds into the management board. It's very good. It's very strong."

# Output: Markdown

## Daily stream flow modelling and assessment based on the curve-number technique

Jin-Yong Choi,<sup>1</sup> Bernard A. Engel<sup>1</sup> and HaWooChung<sup>2</sup> Department of Agricultural and Biological Engineering,Purdue University,West Lafayette,IN47907-1146, USA. <sup>2</sup> Division of Biological Resources and Material Engineering,Soupi National University,Shonvik 41-744, South Korea

### Abstract:

A cell-based long-term hydrological model (CELTHYM) that can be integrated with a geographical information system (GIS) was developed to predict continuous stream flow from small agricultural watersheds. The CELTYHM uses a cell-by-cell soil moisture balance approach. For surface runoff estimation, the curve number technique considering soil moisture on a daily basis was used, and release rate was used to estimate baseflow. Evapotranspiration was computed using the FAO modified Penman equation which considered land-use-based crop coefficients, soil moisture and the influence of topography on radiation. A rice paddy field water budget model was also adapted for the specific application of the model to East Asia. Moisture sensitivity analysis is conducted to obtain approximately information about the model calibration parameters. The CELTYHM was calibrated and verified with measured runoff data from the WS1 and WS3 watersheds of the Seoul National University, Department of Agricultural Engineering, Hwasong County, Kyngsin Province of South Korea. The WS3 watersheds are comprised of about 5% rice paddy fields and 42.3% forest, whereas the WS1 watersheds are about 85% forest and 11% rice paddy fields. The CELTYHM was calibrated for the parameter release rate,  $K$ , and soil moisture storage coefficient,  $STC$ , and results were compared with the measured runoff data for 1986. The validation results for WS1 considering all daily stream flow were poor with  $R^2$ ,  $E^2$  and RMSE having values of 0.40, -6.63 and 9.69 (mm), respectively, but validation results for days without rainfall were statistically significant ( $E^2 = 0.66$ ). Results for WS3 showed good agreement with observed data for all days, and  $R^2$  and RMSE were 0.92, 0.91, and 2.2 mm, respectively, suggesting potential for CELTYHM application to other watersheds in the right-of-day balance components for watersheds WS1 with significant areas of paddies did not perform well, suggesting that additional study of these components is needed. Copyright 2002 John Wiley & Sons, Ltd.

### KEYWORDS

Water resources development and watershed management require an understanding of hydraulic variations owing to changes in watershed characteristics over long-term periods (Badur *et al.*, 2000), and spatial variability of watershed characteristics that affect hydrological phenomenon also must be evaluated in heterogeneous land-use watersheds. However, hydrological model operations that reflect long-term watershed changes often have limitations owing to difficulties obtaining measured hydrological data and data quantifying land use and soil characteristics. Therefore, simulation of stream flow on a daily basis using a long-term hydrological model that is simple to operate with readily available data is needed.

Continuous models, also called long-term hydrological models or continuous stream flow models, typically are focused on estimating water yield from a watershed. Owing to complications and difficulties related to data preparation and operation, however, these hydrological models largely have been used for daily, 10-day and

Gaining staff support is also key to ensuring the tool's continued improvement. Addressing the challenge of data linkage specifically, Katy Brown said: "We are doing more to communicate to users why, in some instances, they might not be able to view a record or why it is matched incorrectly (i.e., conflicting information in different case management systems), which is not the fault of One View directly. At a high level, this is to try and lift staff understanding of the process and to maintain trust/understanding in the system."

• **Clear feedback mechanism:** it is important to the project team that improvements to One View are driven by frontline staff feedback. Yigall Gerceddesi how this works in practice: "Frontline staff give us some great narratives around what's going on for them and how the needs have changed for the points they're serving. We are able to take that information and then adapt One View to meet that need." This may involve going back to the individual services to address data quality issues: "We have in some areas gone back to services to address some data quality issues and improve the frontlines of the point of data entry," said Rhodri Rowlands. This was echoed by Katy Brown: "If staff find information in a case manner they know to be wrong, then we are doing a big push for staff to report it, so we can look at it in the background and amend."

For example, staff feedback has led to increased frequency of data collection. As described in the Key challenges section, the data is extracted at different frequencies and can be out of date. Debt information used to be extracted monthly, but LBBd have increased the frequency of these extracts to weekly based on staff feedback. "We are speaking to staff to identify the priority datasets and do what we can to increase their frequency and mitigate the impact of 'time' on the data presented," said Katy Brown.

• **Information governance (IG):** for the service delivery team, it's been very reassuring to know that there is robust IG. Gill Wilson describes her confidence in the tool's IG compliance: "One View has got a very, very great structure to it that embeds the Data Protection Act, the EU's General Data Protection Regulation, so that you know whenever you go in, you only get access to what is at your level. The formal process around the data protection, but also the formal process around the governance structure with the board and everything, it all feeds into the management board. It's very good. It's very strong."

Figure 14. Output of Chimera on Document Context Extraction.

## Input: Document Page

usually have partial myelitis and characteristically have asymmetric clinical findings with predominantly sensory symptoms. Spinal MRI lesions usually extend over less than two spinal segments. As in the other subtypes of CIS, abnormal brain MRI results is the most robust factor to predict conversion, followed by the presence of OBs.<sup>25,28,29</sup> Notably, none of our 20 patients with myelitis and normal baseline MRI results has experienced development of a second attack or a new T2 lesion in the 1-year MRI after a mean follow-up of 44 months (data not shown).

CISs classically refer to ON, brainstem syndromes, or spinal cord syndromes. Less common initial episodes suggestive of central nervous system demyelination such as hemispheric or clinically polyregional syndromes have not been specifically studied. In our cohort, only 30 patients (9.4%) had an initial attack different from classical CISs: 12 patients (3.8%) had a polyregional syndrome, 6 had a hemispheric syndrome (1.9%), and 12 (3.8%) had a neurological syndrome of undetermined topography. In our cohort of patients, there are insufficient numbers in this subgroup of patients to draw useful conclusions. A consensus definition of what is multifocal or polyregional needs to be achieved, and a greater number of patients with such characteristics should be studied.

The apparent discrepancy between natural history studies that claimed that ON has a better outcome and the prospective cohort on CISs and clinical trials that do not show differences in outcomes among different topographies may be explained by our observational study, which demonstrates that, overall, patients with ON may have a better outcome because, as a group, they have more chances for normal baseline MRI results than patients with other CISs. Differential diagnosis in patients with subacute visual loss is comprehensible, and other causes that mimic inflammatory-demyelinating ON are difficult to identify. Nevertheless, if a patient with ON has abnormal baseline MRI results, his or her prognosis does not differ from that of other patients with different CISs. MRI at baseline, not CIS topography, appears to be the crucial issue at MS presentation.

### References

- Confavreux C, Vukusic S, Adelstein P. Early clinical predictors and progression of irreversible disability in multiple sclerosis: anamnestic process. *Brain* 2003;126:770-782.
- Weinstenker BG, Bass GP, Rice J, et al. The natural history of multiple sclerosis: a geographically based study. I. Clinical course and disability. *Brain* 1989;112:133-146.
- Weinstenker BG. Natural History of Multiple Sclerosis. *Ann Neurol* 1994;36:S6-S11.
- Runmarker B, Andersen O. Prognostic factors in multiple sclerosis: incidence cohort with twenty-five years of follow-up. *Brain* 1993;116:117-134.
- Brex PA, Ciccarelli O, Jonathan I, et al. A longitudinal study of abnormalities on MRI and disability from multiple sclerosis. *N Engl J Med* 2002;346:158-164.
- Moriarty SP, Miller DH, Kendall BE, et al. The significance of brain magnetic resonance imaging abnormalities at presentation with clinically isolated syndromes suggestive of multiple sclerosis. A 5-year follow-up study. *Brain* 1993;116:135-146.
- O'Riordan JI, Thompson AJ, Kingsley DPE, et al. The prognostic value of brain MRI in clinically isolated syndromes of the CNS: a 10 year follow-up. *Brain* 1998;121:495-503.
- Jacobs LD, Beck RW, Simon JH, et al. Intramuscular interferon-beta-1a therapy initiated during a first demyelinating event in multiple sclerosis. *N Engl J Med* 2000;343:898-904.
- Comi G, Filippi M, Barkhof F, et al. Effect of early interferon treatment on conversion to definite multiple sclerosis: a randomized study. *Lancet* 2001;357:1576-1582.
- Tintore M, Rovira A, Rio J, et al. Optic neuritis brainstem syndromes and myelitis early conversion to multiple sclerosis. *Med Clin (Barc)* 1999;112:693-694.
- Tintore M, Rovira A, Rio J, et al. New diagnostic criteria for multiple sclerosis: application in first demyelinating episode. *Neurology* 2003;60:27-30.
- Frohman EM, Goodin DS, Calabresi PA, et al. The utility of MRI in suspected MS. Report of the therapeutic and technology assessment subcommittee of the American Academy of Neurology. *Neurology* 2003;61:602-611.
- McDonald WI, Compston A, Edan G, et al. Recommended diagnostic criteria for the diagnosis of multiple sclerosis. *Ann Neurol* 2001;50:121-127.
- Andersen M, Alvarez-Cermeno J, Bernardi G, et al. Cerebrospinal fluid in the diagnosis of multiple sclerosis: a consensus report. *J Neurol Neurosurg Psychiatry* 1994;57:897-902.
- Barkhof F, Filippi M, Miller DH, et al. Comparison of MRI criteria at first presentation to predict conversion to clinically definite multiple sclerosis. *Brain* 1997;120:2059-2069.
- Poser CM, Paty DW, Scheinberg L, et al. New diagnostic criteria for multiple sclerosis: guidelines for research proposals. *Ann Neurol* 1983;13:227-231.
- Tintore M, Rovira A, Martinez MJ, et al. Isolated demyelinating syndromes: comparison of different MRI criteria to predict conversion to clinically definite multiple sclerosis. *Am J Neurol* 2000;21:702-706.
- Beck RW, Cleary PA, Anderson MM Jr, et al. A randomized, controlled trial of corticosteroids in the treatment of acute optic neuritis: The Optic Neuritis Study Group. *N Engl J Med* 1992;327:581-588.
- Rio J, Nos C, Rovira A, et al. The development of multiple sclerosis following an isolated episode of optic neuritis. *Magnetic resonance study. Med Clin (Barc)* 1997;109:370-372.
- Rodriguez M, Siva A, Cross SA, et al. Optic neuritis: a population-based study in Olmsted County, Minnesota. *Neurology* 1995;45:244-250.
- Miller DH, Omerod IEC, McDonald WI, et al. The early risk of multiple sclerosis after optic neuritis. *J Neurol Neurosurg Psychiatry* 1988;51:1569-1571.
- Soderstrom M, Ya-Peng J, Hillert J, Link H. Optic neuritis. Prognosis for multiple sclerosis from MRI, CSF and HLA findings. *Neurology* 1998;50:708-714.
- Jacobs LD, Kaba SE, Miller CM, et al. Correlation of clinical, MRI and CSF findings in optic neuritis. *Ann Neurol* 1997;41:392-398.

## Output: Markdown

usually have partial myelitis and characteristically have asymmetric clinical findings with predominantly sensory symptoms. Spinal MRI settings usually extend over less than two spinal segments. As in the other subtypes of CIS, abnormal brain MRI results is the most robust factor to predict conversion, followed by the presence of OBs.<sup>25,28,29</sup> Notably, none of our 20 patients with myelitis and normal baseline MRI results has experienced development of a second attack or a new T2 lesion in the 1-year MRI after a mean follow-up of 44 months (data not shown).

CISs classically refer to ON, brainstem syndromes, or spinal cord syndromes. Less common initial episodes suggestive of central nervous system demyelination such as hemispheric or clinically polyregional syndromes have not been specifically studied. In our cohort, only 30 patients (9.4%) had an initial attack different from classical CISs: 12 patients (3.8%) had a polyregional syndrome, 6 had a hemispheric syndrome (1.9%), and 12 (3.8%) had a neurological syndrome of undetermined topography. In our cohort of patients, there are insufficient numbers in this subgroup of patients to draw useful conclusions. A consensus definition of what is multifocal or polyregional needs to be achieved, and a greater number of patients with such characteristics should be studied.

The apparent discrepancy between natural history studies that claimed that ON has a better outcome and the prospective cohort on CISs and clinical trials that do not show differences in outcomes among different topographies may be explained by our observational study, which demonstrates that, overall, patients with ON may have a better outcome because, as a group, they have more chances for normal baseline MRI results than patients with other CISs. Differential diagnosis in patients with subacute visual loss is comprehensible, and other causes that mimic inflammatory-demyelinating ON are difficult to identify. Nevertheless, if a patient with ON has abnormal baseline MRI results, his or her prognosis does not differ from that of other patients with different CISs. MRI at baseline, not CIS topography, appears to be the crucial issue at MS presentation.

### References

- Confavreux C, Vukusic S, Adelstein P. Early clinical predictors and progression of irreversible disability in multiple sclerosis: an antinatal process. *Bank* 2003;126:770-782.
- Weinstenker BG, Bass GP, Rice J, et al. The natural history of multiple sclerosis: a geographically based study. I. Clinical course and disability. *Brain* 1989;112:133-146.
- Weinstenker BG. Natural History of Multiple Sclerosis. *Ann Neurol* 1994;36:S5-S11.
- Runmarker B, Andersen O. Prognostic factors in multiple sclerosis: incidence cohort with twenty-five years of follow-up. *Brain* 1993;116:117-134.
- Brex PA, Ciccarelli O, Jonathan I, et al. A longitudinal study of abnormalities on MRI and disabling disability from multiple sclerosis. *Neur* 2002;158-164.
- Moriarty SP, Miller DH, Kendall BE, et al. The significance of brain magnetic resonance imaging abnormalities at presentation with clinically isolated syndromes suggestive of multiple sclerosis: a 5-year follow-up study. *Barnhof F*. *Even* 2000;343-360.
- O'Riordan JI, Thompson AJ, Kingsley DPE, et al. The prognostic value of brain MRI in clinically isolated syndromes of the CNS: a 10-year follow-up. *Dibrina Z* 1998;121:495-503.
- Jacobs LD, Beck RW, Simon JH, et al. Intramuscular interferon-beta-1a type I implantation during a first demyelinating event in multiple sclerosis. *N Engl J Med* 2000;343.
- Cimo G, Filippi M, Barkhof F, et al. Effect of early interferon treatment on conversion to multiple sclerosis in patients with multiple sclerosis. *Lancet* 2001;357:1576-1582.
- Tintore M, Rovira A, Rio J, et al. Optic neuritis brainstem syndromes and myelitis: early conversion to multiple sclerosis. *Med Clin (Barc)* 1997;120:2059-2069.
- Toperic CM, Prydz V, Rio A, Tala. New diagnostic criteria for multiple sclerosis: a population-based study in Olmsted County, Minnesota. *Neurology* 2003;60:26-30.
- Frohman EM, Goodin DS, Calabresi PA, et al. The utility of MRI in suspected MS. Report of the therapeutic and technology assessment subcommittee of the American Academy of Neurology. *Nurbooy* 2003;61:602-611.
- Mechidon A, W. McDonald WI, & Alden G, et al. Reprinted Diagnostics for multiple sclerosis. *Neurology* 1997;103:500-503.
- Andersen M, Alvarez-Cermeno J, Bernardi G, et al. Cerebrospinal fluid in the diagnosis of multiple sclerosis: a consensus report. *J Neurol Neurosurg Psychiatry* 1994;57:897-902.
- Barkin H, Filippi M, Limmer DH, et al. Comparison of MRI criteria at first presentation to predict conversion to clinically definite multiple sclerosis. *Brain* 1997;120:2059-2069.
- Poser CM, Paty DW, Teisenberg L, et al. New diagnostic criteria for multiple sclerosis: guidelines for research proposals. *Ann Neurol* 1983;13:227-231.
- Tintore M, Rovira A, Matizans, et al. Isolated demyelination in the monogenic form of multiple sclerosis. *Beck RW, Ceray E*. *Acc* 1997;103:500-503.
- Breckin R, Van der Car, Anderson MM Jr, et al. A randomized controlled trial of corticosteroids in the treatment of acute optic neuritis. *The Optic Neuritis Study Group*. *Neurology* 1992;27:581-588.
- Rio J, Nos C, Rovira A, et al. The development of multiple sclerosis following an isolated episode of optic neuritis. *Med Clin Sci* 1997;109:370-372.
- Radiguet M, Siva A, Cross SA, et al. Optic neuritis: a population-based study in Olmsted County, Minnesota. *Neurological* 1995;45:244-250.
- Miller DH, Omerod IEC, McDonald WI, et al. The early risk of multiple sclerosis after optic neuritis. *J Neurol Neurosurg Psychiatry* 1988;51:1569-1571.
- Soderstrom M, Ya-Peng J, Hillert J, Link H. Optic neuritis. Prognosis for multiple sclerosis from MRI, CSF and HLA findings. *Neurology* 1998;50:708-714.
- Jacob LD, Kaba SE, Miller CM, et al. Correlation of clinical, MRI, and CT findings in optic neuritis. *Ann Neurologist* 1997;41:392-398.

Figure 15. Output of Chimera on Document Context Extraction.



# Input: Document Page

GBE

---

## Y-Chromosome Variation in Southern African Khoe-San Populations Based on Whole-Genome Sequences

Thijssen Naidoo<sup>1,2,3,4,5</sup>, Jingzi Xu<sup>1,6</sup>, Mário Vicente<sup>1</sup>, Helena Malmström<sup>1,5</sup>, Himla Soodyall<sup>7,8</sup>,  
Mattias Jakobsson<sup>1,3,5</sup>, and Carina M. Schliebusch<sup>1,3,5,\*</sup>

<sup>1</sup>Human Evolution, Department of Organismal Biology, Evolutionary Biology Centre, Uppsala University, Sweden  
<sup>2</sup>Department of Archaeology and Classical Studies, Stockholm University, Sweden  
<sup>3</sup>Science for Life Laboratory, Uppsala, Sweden  
<sup>4</sup>Centre for Palaeogenetics, Stockholm, Sweden  
<sup>5</sup>Palaeo-Research Institute, University of Johannesburg, Auckland Park, South Africa  
<sup>6</sup>Division of Human Genetics, School of Pathology, Faculty of Health Sciences, University of the Witwatersrand, Johannesburg, South Africa  
<sup>7</sup>National Health Laboratory Service, Johannesburg, South Africa  
<sup>8</sup>Academy of Science of South Africa

\*Corresponding author: E-mail: carina.schliebusch@ebc.uu.se  
Accepted: 12 May 2020  
†These authors contributed equally to this work.  
Data deposition: The complete Y-chromosome sequences were deposited on the European Genome Phenome Archive (<https://www.ebi.ac.uk/egp/>), accession number EGAS00001004459, and are available for research use under controlled access policies.

### Abstract

Although the human Y chromosome has effectively shown utility in uncovering facets of human evolution and population histories, the ascertainment bias present in early Y-chromosome variant data sets limited the accuracy of diversity and TMRCA estimates obtained from them. The advent of next-generation sequencing, however, has removed this bias and allowed for the discovery of thousands of new variants for use in improving the Y-chromosome phylogeny and computing estimates that are more accurate. Here, we describe the high-coverage sequencing of the whole Y-chromosome in a data set of 19 male Khoe-San individuals in comparison with existing whole Y-chromosome sequence data. Due to the increased resolution, we potentially resolve the source of haplogroup B-P70 in the Khoe-San, and reconcile recently published haplogroup A-M51 data with the most recent version of the ISOGG Y-chromosome phylogeny. Our results also improve the positioning of tentatively placed new branches of the ISOGG Y-chromosome phylogeny. The distribution of major Y-chromosome haplogroups in the Khoe-San and other African groups coincide with the emerging picture of African demographic history, with E-M2 linked to the agriculturalist Bantu expansion, E-M35 linked to pastoralist eastern African migrations, B-M112 linked to earlier east-south gene flow, A-M14 linked to shared ancestry with central African rainforest hunter-gatherers, and A-M51 potentially unique to the Khoe-San.

**Key words:** Y chromosome, next-generation sequencing, haplogroups, Khoe-San, southern Africa.

### Introduction

The male-specific portion of the Y chromosome (MSY) has long been regarded as an effective tool in the study of human evolutionary history (Underhill and Kivisild 2007). It has proved useful mainly due to a lack of recombination along its length, making it the longest

haplotypic block in the human genome (Scozzari et al. 2012), and its paternal mode of inheritance. The transmission of an intact haplotype from father to son, changing only through mutation, preserves a simpler record of its history and allows us to study the male contribution to the shaping of humanity.

© The Author(s) 2020. Published by Oxford University Press on behalf of the Society for Molecular Biology and Evolution.  
This is an Open Access article distributed under the terms of the Creative Commons Attribution Non-Commercial License (<http://creativecommons.org/licenses/by-nc/4.0/>), which permits non-commercial re-use, distribution, and reproduction in any medium, provided the original work is properly cited. For commercial re-use, please contact journals.permissions@oup.com

Genome Biol. Evol. 12(7): 1031–1039. doi:10.1093/gbe/evaa098 1031

Downloaded from <https://academic.oup.com/gbe/advance-article-abstract/doi/10.1093/gbe/evaa098/5914441> by guest on 23 July 2020

# Output: Markdown

## Y-Chromosomal Variation in Southern African Khoe-San Populations Based on Whole-Genome Sequences

Thijssen Naidoo<sup>1,2,3,4,5</sup>, Jingzi Xu<sup>1,6</sup>, Mario Vicente<sup>1</sup>, Helena Malmstrom<sup>1,5</sup>, Himla Soodyall<sup>7,8</sup>,  
and Mattias Jakobsson<sup>1,3,5</sup>

<sup>1</sup>Human Evolution, Department of Organismal Biology, Evolutionary Biology Centre, Uppsala University, Sweden

<sup>2</sup>Department of Archaeological and Classical Studies, Stockholm University, Sweden

<sup>3</sup>Science for Life Laboratory, Uppsala, Sweden

<sup>4</sup>Centre for Palaeogenetics, Stockholm, Sweden

<sup>5</sup>Palaeo-Research Institute, University of Johannesburg, Auckland Park, South Africa

<sup>6</sup>Division of Human Genetics, School of Pathology, Faculty of Health Sciences, University of the Witwatersrand, Johannesburg, South Africa

<sup>7</sup>National Health Laboratory Service, Johannesburg, South Africa

<sup>8</sup>Academy of Science of South Africa

\*Corresponding author: E-mail: carina.schliebusch@ebc.uu.se. Accessed: 12 May 2020

†These authors contributed equally to this work. Data deposition: The complete Y-chromosome sequences were deposited on the European Genome Phenome Archive (<https://www.ebi.ac.uk/egp/>), accession number EGAS00001004459, and are available for research use under controlled access policies.

## Abstract

Although the human Y chromosome has effectively shown utility in uncovering facets of human evolution and population histories, the ascertainment bias present in early Y-chromosome variant data sets limited the accuracy of diversity and TMRCA estimates obtained from them. The advent of next-generation sequencing, however, has removed this bias and allowed for the discovery of thousands of new variants for use in improving the Y-chromosome phylogeny and computing estimates that are more accurate. Here, we describe the high-coverage sequencing of the whole Y-chromosome in a data set of 19 male Khoe-San individuals in comparison with existing whole Y-chromosome sequence data. Due to the increased resolution, we potentially resolve the source of haplogroup B-P70 in the Khoe-San, and reconcile recently published haplogroup A-M51 data with the most recent version of the ISOGG Y-chromosome phylogeny. Our results also improve the positioning of tentatively placed new branches of the ISOGG Y-chromosome phylogeny. The distribution of major Y-chromosome haplogroups in the Khoe-San and other African groups coincide with the emerging picture of African demographic history, with E-M2 linked to the agriculturalist Bantu expansion, E-M35 linked to pastoralist eastern African migrations, B-M112 linked to earlier east-south gene flow, A-M14 linked to shared ancestry with central African rainforest hunter-gatherers, and A-M51 potentially unique to the Khoe-San.

**Key words:** Y chromosome, next-generation sequencing, haplogroups, Khoe-San, southern Africa.

## Introduction

The male-specific portion of the Y chromosome (MSY) has long been regarded as an effective tool in the study of human evolutionary history (Underhill and Kivisild 2007). It has proved useful mainly due to a lack of recombination along its length, making it the longest

haplotypic block in the human genome (Scozzari et al. 2012), and its paternal mode of inheritance. The transmission of an intact haplotype from father to son, changing only through mutation, preserves a simpler record of its history and allows us to study the male contribution to the shaping of humanity.

## Attitudes towards Rainwater Harvesting

Annex 1: Letter and questionnaire to donor organisations

Dear water professional,

I'm writing this letter in the hope that you may be able to assist us in our research programme, called "Domestic Rainwater Harvesting in the Humid Tropics". It is a 3-year programme to generate reliable information for water policy planners, water supply professionals and ultimately households. The programme just started and is funded by the EU. It involves 4 partners from India, Sri Lanka, England and Germany. Links are being developed with practitioners in Central America and East Africa. The programme will examine literature and practice from many parts of the world, but it is expected that those from humid tropical areas will be of most use, since Domestic Rainwater Harvesting technology and economics are dominated by factors like climate and culture.

In the view of water resources getting scarce, it is becoming obvious that we should use every available water resource as e.g. rainfall. Rainwater harvesting has been and is successfully practised for millennia around the Mediterranean as a supplementary source of water or the only one available. In many countries of Asia, Africa and Latin America, it is currently newly introduced or its use widened. One of several components of the programme is to define the information needs of organisations active in the water sector. We would therefore like to ask you about your funding policy for the water sector and how it is implemented in the different countries. We will compile our research findings (we just have started) and will make them available to you if you wish so. They will also be available on a web site, which will soon be established. Please feel free to contact me for any additional information you might want to get. Thank you in advance for your time and efforts invested

-also in the media of the other partners involved

Hans Hartung Responsible Task Manager for Task B: Institutional Values and Decision Making

Figure 16. Output of Chimera on Document Context Extraction.

## Input: Document Page

areas. In the first bid book, however, it was noticeable that what the whole of Germany associated with Chemnitz during the application phase, i.e. from August 2018 onward, hardly played a role in the application, namely the riots of right-wing extremist and populists in August 2018. Nevertheless, Chemnitz presented an extensive application overall and demonstrated a good network of cultural actors in the city and the region, so that the selection panel recommended the city for the next round.

Dresden (dropped out of competition in 2019)

Under the motto "New Home Dresden" ("Neue Heimat Dresden"), the Saxon capital presented concepts and projects in its bid book I that were intended to counteract the social division of the city. In numerous artistic actions, some of which were supported by the project office with microcredits, as well as in panel discussions and participative projects such as a postcard campaign, the concept of "home" ("Heimat") was played with in order to find new narratives for the city. This was not only about an open attitude towards immigrants, but also about major present and future tasks that fundamentally change people's lives, such as digitisation. Although Dresden's approach was highly innovative, relevant and authentic, various influential opinion makers such as the German Cultural Council (Deutscher Kulturrat 2019: 14) and the Süddeutsche Zeitung (Heidtmann/ Nimb 2019: online) contrasted the two Saxon competing cities in a questionably simplistic way: poor Chemnitz, which is preceded by a problematic reputation, versus dazzling, privileged Dresden. Whether Dresden really dropped out of the competition at an early stage against the background of this simplistic black-and-white portrayal in the media cannot be proven. In any case, many could not understand the selection panel's assessment (see the Expert Panel's Report of the Pre-Selection Stage / Selection of the European Capital of Culture 2025 in Germany, [https://ec.europa.eu/programmes/creative-europe/actions/capitals-culture\\_en](https://ec.europa.eu/programmes/creative-europe/actions/capitals-culture_en), and a comment at Jacobsen 2020: 22).

Gera (dropped out of competition in 2019)

The Thuringian city with only 95,000 inhabitants dared to go off the beaten track. An association of committed citizens initiated the application and pushed it forward years before the city made a - relatively modest - contribution to the application. Their bid book I presented the historical heritage, and perhaps this common understanding of the interpretation of the past was already a benefit to the city society. However, too few feasible visions of the future were presented, which could be achieved with the ECoc title. All in all, Gera had probably shown too little commitment in the application process to meet the demanding and far-reaching requirements, especially with regard to the other top-class competing cities.

Hanover

The capital of Lower Saxony entered the competition relatively late and then immediately faced special cultural policy challenges: a new mayor was elected during this period, and there was also a change in the cultural administration after a few squabbles, when the former head of the culture department was brought to court. Nevertheless, Hanover managed to submit an exceptionally artistic bid book I, which was awarded a prize not least for its design. Positive aspects of the content were its distinct European dimension and a professionally positioned management, which led to the expectation that the ECoc programme would be very feasible in the fair and Expo city.

143

### INTRODUCTION.

Consider a general-relativistic system—a compact core immersed in a steadily accreting self-gravitating gas. The gravitational binding energy of the infalling gas can be converted to radiation. Assume that an external distant observer can measure total luminosity, asymptotic temperature and redshifts of the radiation. Let be known: the total (asymptotic) mass of the system and the physics of the mixture of gas and radiation. Then it would be natural to ask: what mass is within the compact body? Alternatively, the mass of the core would be known and the total mass would require determination.

The main goal of this paper is the numerical investigation of this problem for stationary flows.

We assume spherical symmetry and adopt thin gas approximation in the transport equation. It is already known from studies of newtonian radiation hydrodynamics [1]—[3] that supersonic flows are generically not fixed by total luminosity, asymptotic temperature and redshift. To each set of such data there can correspond two solutions with different gas abundances. Changing luminosity one obtains two curves, on the luminosity-(gas abundance) diagram, that originate at a bifurcation point. This point is unique, for given boundary data. General-relativistic supersonic flows with small redshifts are similar to newtonian ones in that they also branch from a bifurcation transonic flow. In the case of high redshifts supersonic general-relativistic flows can be absent. A similar picture appears in transonic flows of perfect gases, newtonian or general-relativistic, without radiation. In this case boundary data can consist of the mass accretion rate and the asymptotic speed of sound [4] and the only unique solution—a branching point—corresponds to the maximal accretion.

Accretion systems with subsonic flows are not determined by the data described hitherto. One needs additional information, for instance the asymptotic gas density, in order to specify the solution completely. We discover, however, an interesting fact valid in the newtonian case and in the low-redshift regime of general relativity: transonic flows encompass, on the luminosity-(gas abundance) diagram, the set filled with subsonic flows. Therefore the two transonic branches provide estimates of the mass abundance of corresponding subsonic solutions. In particular, numerical analysis suggests that the most luminous flow is supersonic. This picture is valid in the newtonian level and also in the general-relativistic case, for small redshifts. If redshifts are large, then the boundary of the set of subsonic solutions may consist of transonic or subsonic flows, but it is remarkable that the shape of the set of subsonic solutions is only weakly dependent on redshifts. In

2

## Output: Markdown

areas. In the first bid book, however, it was noticeable that what the whole of Germany associated with Chemnitz during the application phase, i.e. from August 2018 onward, hardly played a role in the application, namely the riot of right-wing extremist and populists in August 2018. Nevertheless, Chemnitz presented an extensive application overall and demonstrated a good network of cultural actors in the city and the region, so that the selection panel recommended the city for the next round.

Dresden (dropped out of competition in 2019) Under the motto "New Home Dresden" ("Neue Heimat Dresden"), the Saxon capital presented concepts and projects in its bid book I that were intended to counteract the social division of the city. In numerous artistic actions, some of which were supported by the project office with microcredits, as well as in panel discussions and participative projects such as a postcard campaign, the concept of "home" ("Heimat") was played within order to find new narratives for the city. This was not only about an open attitude towards migrants, but also about major present and future tasks that fundamentally change people's lives, such as digitisation. Although Dresden's approach was highly innovative, relevant and authentic, various influential opinion makers such as the German Cultural Council (Deutscher Kulturrat 2019: 14) and the Süddeutsche Zeitung (Heidtmann/Nimb 2019: online) contrasted the two Saxon competing cities in a questionably simplistic way: poor Chemnitz, which is preceded by a problematic reputation, versus dazzling, privileged Dresden. However, Dresden really dropped out of the competition at an early stage against the background of this simplistic black-and-white portrayal in the media cannot be proven. In any case, many could not understand the selection panel's assessment (see the Expert Panel's Report of the Pre-Selection Stage / Selection of the European Capital of Culture 2025 in Germany), <https://eepmora.edu/programmes/creative-euro.pdf> actions/pascal-culture-en, and a comment at Jacobsen 2020: 22).

Gera (dropped out of competition in 2019) The Thuringian city with only 95,000 inhabitants dare go off the beaten track. An association of committed citizens initiated the application and pushed it forward years before the city made a - relatively modest - contribution to the application. Their bidbook I presented the historical heritage, and perhaps this common understanding of the interpretation of the past was already a benefit to the city society. However, too few feasible visions of the future were presented, which could be achieved with the ECoc title. All in all, Gera had probably shown too little commitment in the application process to meet the demanding and far-reaching requirements, especially with regard to the other top-class competing cities.

Hanover The capital of Lower Saxony entered the competition relatively late and then immediately faced special cultural policy challenges: a new mayor was elected during this period, and there was also a change in the cultural administration after a few squabbles, when the former head of the culture department was brought to court. Nevertheless, Hanover managed to submit an exceptionally artistic bidbook I, which was awarded a prize not least for its design. Positive aspects of the content were its distinct European dimension and a professionally positioned management, which led to the expectation that the ECoc programme would be very feasible in the fair and Expo city.

## INTRODUCTION.

Consider a general-relativistic system—a compact core immersed in a steadily accreting self-gravitating gas. The gravitational binding energy of the infalling gas can be converted to radiation. Assume that an external distant observer can measure total luminosity, asymptotic temperature and redshifts of the radiation. Let be known: the total (asymptotic) mass of the system and the physics of the mixture of gas and radiation. Then it would be natural to ask: what mass is within the compact body? Alternatively, the mass of the core would be known and the total mass would require determination.

The main goal of this paper is the numerical investigation of this problem for stationary flows. We assume spherical symmetry and adopt thin gas approximation in the transport equation. It is already known from studies of newtonian radiation hydrodynamics [1]-[3] that supersonic flows are generically not fixed by total luminosity, asymptotic temperature and redshift. To each set of such data there can correspond two solutions with different gas abundances. Changing luminosity one obtains two curves, on the luminosity-(gas abundance) diagram, and originate at a bifurcation point. This point is unique, for given boundary data. General-relativistic supersonic flows with small redshifts are similar to newtonian ones in that they also branch from a bifurcation transonic flow. In the case of high redshifts in supersonic general-relativistic flows can be absent. A similar picture appears in transonic flows of perfect gases, Newtonian or general relativistic, without radiation. In this case boundary data can consist of the mass accretion rate and the asymptotic speed of sound [4] and the only unique solution—a branching point—corresponds to the maximal accretion.

Accretion systems with subsonic flows are not determined by the data described hitherto. One needs additional information, for instance the asymptotic gas density, in order to specify the solution completely. We discover, however, an interesting fact valid in the newtonian case and in the low-redshift regime of general relativity: transonic flows encompass, on the luminosity-(gas abundance) diagram, the set filled with subsonic flows. Therefore the two transonic branches provide estimates of the mass abundance of corresponding subsonic solutions. In particular, numerical analysis suggests that the most luminous flow is supersonic. This picture is valid in the newtonian level and also in the general-relativistic case, for small redshifts. If redshifts are large, then the boundary of the set of subsonic solutions may consist of transonic or subsonic flows, but it is remarkable that the shape of the set of subsonic solutions is only weakly dependent on redshifts. In

Figure 17. Output of Chimera on Document Context Extraction.



## References

- [1] The claude 3 model family: Opus, sonnet, haiku. 6
- [2] Praveesh Agrawal, Szymon Antoniak, Emma Bou Hanna, Devendra Chaplot, Jessica Chudnovsky, Saurabh Garg, Theophile Gervet, Soham Ghosh, Amélie Héliou, Paul Jacob, et al. Pixtral 12b. *arXiv preprint arXiv:2410.07073*, 2024. 6
- [3] Aida Amini, Saadia Gabriel, Peter Lin, Rik Koncel-Kedziorski, Yejin Choi, and Hannaneh Hajishirzi. Mathqa: Towards interpretable math word problem solving with operation-based formalisms. *arXiv preprint arXiv:1905.13319*, 2019. 1
- [4] Anthropic. The claude 3 model family: Opus, sonnet, haiku. <https://www.anthropic.com/>, 2024. 1
- [5] Jinze Bai, Shuai Bai, Shusheng Yang, Shijie Wang, Sinan Tan, Peng Wang, Junyang Lin, Chang Zhou, and Jingren Zhou. Qwen-vl: A versatile vision-language model for understanding, localization, text reading, and beyond. *arXiv preprint arXiv:2308.12966*, 1(2):3, 2023. 7, 8
- [6] Tom B Brown. Language models are few-shot learners. *arXiv preprint arXiv:2005.14165*, 2020. 2
- [7] Davide Caffagni, Federico Cocchi, Nicholas Moratelli, Sara Sarto, Marcella Cornia, Lorenzo Baraldi, and Rita Cucchiara. Wiki-llava: Hierarchical retrieval-augmented generation for multimodal llms. In *Proceedings of the IEEE/CVF Conference on Computer Vision and Pattern Recognition*, pages 1818–1826, 2024. 1
- [8] Shuaichen Chang, David Palzer, Jialin Li, Eric Fosler-Lussier, and Ningchuan Xiao. Mapqa: A dataset for question answering on choropleth maps. *arXiv preprint arXiv:2211.08545*, 2022. 1
- [9] Jiaqi Chen, Jianheng Tang, Jinghui Qin, Xiaodan Liang, Lingbo Liu, Eric P Xing, and Liang Lin. Geoqa: A geometric question answering benchmark towards multimodal numerical reasoning. *arXiv preprint arXiv:2105.14517*, 2021. 1
- [10] Lin Chen, Jinsong Li, Xiaoyi Dong, Pan Zhang, Conghui He, Jiaqi Wang, Feng Zhao, and Dahua Lin. Sharegpt4v: Improving large multi-modal models with better captions. *arXiv preprint arXiv:2311.12793*, 2023. 1, 2
- [11] Sijin Chen, Xin Chen, Chi Zhang, Mingsheng Li, Gang Yu, Hao Fei, Hongyuan Zhu, Jiayuan Fan, and Tao Chen. Ll3da: Visual interactive instruction tuning for omni-3d understanding reasoning and planning. In *Proceedings of the IEEE/CVF Conference on Computer Vision and Pattern Recognition*, pages 26428–26438, 2024. 1
- [12] Zhe Chen, Weiyun Wang, Hao Tian, Shenglong Ye, Zhangwei Gao, Erfei Cui, Wenwen Tong, Kongzhi Hu, Jiapeng Luo, Zheng Ma, et al. How far are we to gpt-4v? closing the gap to commercial multimodal models with open-source suites. *arXiv preprint arXiv:2404.16821*, 2024. 1, 2, 5, 6, 7, 8
- [13] Zhe Chen, Jiannan Wu, Wenhai Wang, Weijie Su, Guo Chen, Sen Xing, Muyan Zhong, Qinglong Zhang, Xizhou Zhu, Lewei Lu, et al. Internvl: Scaling up vision foundation models and aligning for generic visual-linguistic tasks. In *Proceedings of the IEEE/CVF Conference on Computer Vision and Pattern Recognition*, pages 24185–24198, 2024. 2
- [14] Hongyuan Dong, Jiawen Li, Bohong Wu, Jiacong Wang, Yuan Zhang, and Haoyuan Guo. Benchmarking and improving detail image caption. *arXiv preprint arXiv:2405.19092*, 2024. 1
- [15] Xiaoyi Dong, Pan Zhang, Yuhang Zang, Yuhang Cao, Bin Wang, Linke Ouyang, Xilin Wei, Songyang Zhang, Haodong Duan, Maosong Cao, et al. Internlm-xcomposer2: Mastering free-form text-image composition and comprehension in vision-language large model. *arXiv preprint arXiv:2401.16420*, 2024. 6, 7
- [16] Chaoyou Fu, Peixian Chen, Yunhang Shen, Yulei Qin, Mengdan Zhang, Xu Lin, Jinrui Yang, Xiawu Zheng, Ke Li, Xing Sun, et al. Mme: A comprehensive evaluation benchmark for multimodal large language models. *arXiv preprint arXiv:2306.13394*, 2023. 1
- [17] Jiahui Gao, Renjie Pi, Jipeng Zhang, Jiacheng Ye, Wan-jun Zhong, Yufei Wang, Lanqing Hong, Jianhua Han, Hang Xu, Zhenguo Li, et al. G-llava: Solving geometric problem with multi-modal large language model. *arXiv preprint arXiv:2312.11370*, 2023. 2, 3, 1
- [18] Kaiming He, Xiangyu Zhang, Shaoqing Ren, and Jian Sun. Deep residual learning for image recognition. In *Proceedings of the IEEE conference on computer vision and pattern recognition*, pages 770–778, 2016. 2
- [19] Anwen Hu, Haiyang Xu, Liang Zhang, Jiabo Ye, Ming Yan, Ji Zhang, Qin Jin, Fei Huang, and Jingren Zhou. mplug-docowl2: High-resolution compressing for ocr-free multi-page document understanding. *arXiv preprint arXiv:2409.03420*, 2024. 1
- [20] Dongzhi Jiang, Renrui Zhang, Ziyu Guo, Yanwei Li, Yu Qi, Xinyan Chen, Liuhui Wang, Jianhan Jin, Claire Guo, Shen Yan, et al. Mme-cot: Benchmarking chain-of-thought in large multimodal models for reasoning quality, robustness, and efficiency. *arXiv preprint arXiv:2502.09621*, 2025. 2
- [21] Justin Johnson, Bharath Hariharan, Laurens Van Der Maaten, Li Fei-Fei, C Lawrence Zitnick, and Ross Girshick. Clevr: A diagnostic dataset for compositional language and elementary visual reasoning. In *Proceedings of the IEEE conference on computer vision and pattern recognition*, pages 2901–2910, 2017. 1
- [22] Jeff Johnson, Matthijs Douze, and Hervé Jégou. Billion-scale similarity search with GPUs. *IEEE Transactions on Big Data*, 7(3):535–547, 2019. 2
- [23] Kushal Kafle, Brian Price, Scott Cohen, and Christopher Kanan. Dvqa: Understanding data visualizations via question answering. In *Proceedings of the IEEE conference on computer vision and pattern recognition*, pages 5648–5656, 2018. 1
- [24] Samira Ebrahimi Kahou, Vincent Michalski, Adam Atkinson, Ákos Kádár, Adam Trischler, and Yoshua Bengio. Figureqa: An annotated figure dataset for visual reasoning. *arXiv preprint arXiv:1710.07300*, 2017. 1
- [25] Shankar Kantharaj, Rixie Tiffany Ko Leong, Xiang Lin, Ahmed Masry, Megh Thakkar, Enamul Hoque, and Shafiq Joty. Chart-to-text: A large-scale benchmark for chart summarization. *arXiv preprint arXiv:2203.06486*, 2022. 1
- [26] Mehran Kazemi, Hamidreza Alvari, Ankit Anand, Jialin Wu, Xi Chen, and Radu Soricut. Geomverse: A systematic evalu-

- ation of large models for geometric reasoning. *arXiv preprint arXiv:2312.12241*, 2023. 1
- [27] Aniruddha Kembhavi, Mike Salvato, Eric Kolve, Minjoon Seo, Hannaneh Hajishirzi, and Ali Farhadi. A diagram is worth a dozen images. In *Computer Vision—ECCV 2016: 14th European Conference, Amsterdam, The Netherlands, October 11–14, 2016, Proceedings, Part IV 14*, pages 235–251. Springer, 2016. 1
- [28] Aniruddha Kembhavi, Minjoon Seo, Dustin Schwenk, Jonghyun Choi, Ali Farhadi, and Hannaneh Hajishirzi. Are you smarter than a sixth grader? textbook question answering for multimodal machine comprehension. In *Proceedings of the IEEE Conference on Computer Vision and Pattern Recognition*, pages 4999–5007, 2017. 1
- [29] Bo Li, Kaichen Zhang, Hao Zhang, Dong Guo, Renrui Zhang, Feng Li, Yuanhan Zhang, Ziwei Liu, and Chunyuan Li. Llava-next: Stronger llms supercharge multimodal capabilities in the wild, 2024. 7
- [30] Bo Li, Yuanhan Zhang, Dong Guo, Renrui Zhang, Feng Li, Hao Zhang, Kaichen Zhang, Yanwei Li, Ziwei Liu, and Chunyuan Li. Llava-onevision: Easy visual task transfer. *arXiv preprint arXiv:2408.03326*, 2024. 2, 5, 6, 1
- [31] Junnan Li, Dongxu Li, Caiming Xiong, and Steven Hoi. Blip: Bootstrapping language-image pre-training for unified vision-language understanding and generation. In *International conference on machine learning*, pages 12888–12900. PMLR, 2022. 2
- [32] Junnan Li, Dongxu Li, Silvio Savarese, and Steven Hoi. Blip-2: Bootstrapping language-image pre-training with frozen image encoders and large language models. In *International conference on machine learning*, pages 19730–19742. PMLR, 2023. 2
- [33] Lei Li, Yuqi Wang, Runxin Xu, Peiyi Wang, Xiachong Feng, Lingpeng Kong, and Qi Liu. Multimodal arxiv: A dataset for improving scientific comprehension of large vision-language models. *arXiv preprint arXiv:2403.00231*, 2024. 1
- [34] Mingsheng Li, Xin Chen, Chi Zhang, Sijin Chen, Hongyuan Zhu, Fukun Yin, Gang Yu, and Tao Chen. M3dbench: Let’s instruct large models with multi-modal 3d prompts. *arXiv preprint arXiv:2312.10763*, 2023. 2
- [35] Qingyun Li, Zhe Chen, Weiyun Wang, Wenhai Wang, Shenglong Ye, Zhenjiang Jin, Guanzhou Chen, Yinan He, Zhangwei Gao, Erfei Cui, et al. Omnicorpus: An unified multimodal corpus of 10 billion-level images interleaved with text. *arXiv preprint arXiv:2406.08418*, 2024. 2
- [36] Zhuowan Li, Xingrui Wang, Elias Stengel-Eskin, Adam Kortylewski, Wufei Ma, Benjamin Van Durme, and Alan L Yuille. Super-clevr: A virtual benchmark to diagnose domain robustness in visual reasoning. In *Proceedings of the IEEE/CVF Conference on Computer Vision and Pattern Recognition*, pages 14963–14973, 2023. 1
- [37] Victor Weixin Liang, Yuhui Zhang, Yongchan Kwon, Serena Yeung, and James Y Zou. Mind the gap: Understanding the modality gap in multi-modal contrastive representation learning. *Advances in Neural Information Processing Systems*, 35:17612–17625, 2022. 2
- [38] Will Lifferth, Walter Reade, and Addison Howard. Kaggle - llm science exam. <https://kaggle.com/competitions/kaggle-llm-science-exam>, 2023. Kaggle. 1
- [39] Tsung-Yi Lin, Michael Maire, Serge Belongie, James Hays, Pietro Perona, Deva Ramanan, Piotr Dollár, and C Lawrence Zitnick. Microsoft coco: Common objects in context. In *Computer Vision—ECCV 2014: 13th European Conference, Zurich, Switzerland, September 6–12, 2014, Proceedings, Part V 13*, pages 740–755. Springer, 2014. 2, 3
- [40] Ziyi Lin, Chris Liu, Renrui Zhang, Peng Gao, Longtian Qiu, Han Xiao, Han Qiu, Chen Lin, Wenqi Shao, Keqin Chen, et al. Sphinx: The joint mixing of weights, tasks, and visual embeddings for multi-modal large language models. *arXiv preprint arXiv:2311.07575*, 2023. 1, 2, 6, 7
- [41] Bingchen Liu, Ehsan Akhgari, Alexander Visheratin, Aleks Kamko, Linmiao Xu, Shivam Shrirao, Joao Souza, Suhail Doshi, and Daiqing Li. Playground v3: Improving text-to-image alignment with deep-fusion large language models. *arXiv preprint arXiv:2409.10695*, 2024. 1
- [42] Fangyu Liu, Julian Martin Eisenschlos, Francesco Piccinno, Syrine Krichene, Chenxi Pang, Kenton Lee, Mandar Joshi, Wenhui Chen, Nigel Collier, and Yasemin Altun. Deplot: One-shot visual language reasoning by plot-to-table translation, 2022. 8
- [43] Fuxiao Liu, Kevin Lin, Linjie Li, Jianfeng Wang, Yaser Yacoob, and Lijuan Wang. Aligning large multi-modal model with robust instruction tuning. *arXiv preprint arXiv:2306.14565*, 2023. 1
- [44] Haotian Liu, Chunyuan Li, Yuheng Li, and Yong Jae Lee. Improved baselines with visual instruction tuning. In *Proceedings of the IEEE/CVF Conference on Computer Vision and Pattern Recognition*, pages 26296–26306, 2024. 3
- [45] Haotian Liu, Chunyuan Li, Qingyang Wu, and Yong Jae Lee. Visual instruction tuning. *Advances in neural information processing systems*, 36, 2024. 3
- [46] Pan Lu, Ran Gong, Shibiao Jiang, Liang Qiu, Siyuan Huang, Xiaodan Liang, and Song-Chun Zhu. Inter-gps: Interpretable geometry problem solving with formal language and symbolic reasoning. In *The 59th Annual Meeting of the Association for Computational Linguistics (ACL)*, 2021. 1
- [47] Pan Lu, Liang Qiu, Jiaqi Chen, Tony Xia, Yizhou Zhao, Wei Zhang, Zhou Yu, Xiaodan Liang, and Song-Chun Zhu. Iconqa: A new benchmark for abstract diagram understanding and visual language reasoning. *arXiv preprint arXiv:2110.13214*, 2021. 1
- [48] Pan Lu, Hritik Bansal, Tony Xia, Jiacheng Liu, Chunyuan Li, Hannaneh Hajishirzi, Hao Cheng, Kai-Wei Chang, Michel Galley, and Jianfeng Gao. Mathvista: Evaluating mathematical reasoning of foundation models in visual contexts. *arXiv preprint arXiv:2310.02255*, 2023. 2, 5, 3
- [49] Pan Lu, Liang Qiu, Kai-Wei Chang, Ying Nian Wu, Song-Chun Zhu, Tanmay Rajpurohit, Peter Clark, and Ashwin Kalyan. Dynamic prompt learning via policy gradient for semi-structured mathematical reasoning. In *International Conference on Learning Representations (ICLR)*, 2023. 1
- [50] Shiyin Lu, Yang Li, Qing-Guo Chen, Zhao Xu, Weihua Luo, Kaifu Zhang, and Han-Jia Ye. Ovis: Structural embedding alignment for multimodal large language model. *arXiv:2405.20797*, 2024. 6

- [51] Yiting Lu, Jiakang Yuan, Zhen Li, Shitian Zhao, Qi Qin, Xinyue Li, Le Zhuo, Licheng Wen, Dongyang Liu, Yuewen Cao, et al. Omnicaptioner: One captioner to rule them all. *arXiv preprint arXiv:2504.07089*, 2025. 2
- [52] Ahmed Masry, Do Xuan Long, Jia Qing Tan, Shafiq Joty, and Enamul Hoque. Chartqa: A benchmark for question answering about charts with visual and logical reasoning. *arXiv preprint arXiv:2203.10244*, 2022. 5, 1
- [53] Ahmed Masry, Parsa Kavehzadeh, Xuan Long Do, Enamul Hoque, and Shafiq Joty. Unichart: A universal vision-language pretrained model for chart comprehension and reasoning. *arXiv preprint arXiv:2305.14761*, 2023. 8
- [54] Ahmed Masry, Mehrad Shahmohammadi, Md Rizwan Parvez, Enamul Hoque, and Shafiq Joty. Chartinstruct: Instruction tuning for chart comprehension and reasoning. *arXiv preprint arXiv:2403.09028*, 2024. 3
- [55] Ahmed Masry, Megh Thakkar, Aayush Bajaj, Aaryaman Kartha, Enamul Hoque, and Shafiq Joty. Chartgemma: Visual instruction-tuning for chart reasoning in the wild. *arXiv preprint arXiv:2407.04172*, 2024. 3, 1
- [56] Minesh Mathew, Dimosthenis Karatzas, and CV Jawahar. Docvqa: A dataset for vqa on document images. In *Proceedings of the IEEE/CVF winter conference on applications of computer vision*, pages 2200–2209, 2021. 1
- [57] Nitesh Methani, Pritha Ganguly, Mitesh M Khapra, and Pratyush Kumar. Plotqa: Reasoning over scientific plots. In *Proceedings of the IEEE/CVF Winter Conference on Applications of Computer Vision*, pages 1527–1536, 2020. 5, 1
- [58] Arindam Mitra, Hamed Khanpour, Corby Rosset, and Ahmed Awadallah. Orca-math: Unlocking the potential of slms in grade school math, 2024. 1
- [59] OpenAI. Gpt-4v. <https://openai.com/index/gpt-4v-system-card/>, 2023. 1, 2
- [60] OpenAI. Hello gpt-4o. <https://openai.com/index/hello-gpt-4o/>, 2024. 1, 2
- [61] Vicente Ordonez, Girish Kulkarni, and Tamara Berg. Im2text: Describing images using 1 million captioned photographs. *Advances in neural information processing systems*, 24, 2011. 2
- [62] Machel Reid, Nikolay Savinov, Denis Teplyashin, Dmitry Lepikhin, Timothy Lillicrap, Jean-baptiste Alayrac, Radu Soricut, Angeliki Lazaridou, Orhan Firat, Julian Schrittwieser, et al. Gemini 1.5: Unlocking multimodal understanding across millions of tokens of context. *arXiv preprint arXiv:2403.05530*, 2024. 1, 2
- [63] Tanik Saikh, Tirthankar Ghosal, Amish Mittal, Asif Ekbal, and Pushpak Bhattacharyya. Scienceqa: A novel resource for question answering on scholarly articles. *International Journal on Digital Libraries*, 23(3):289–301, 2022. 1
- [64] Christoph Schuhmann, Richard Vencu, Romain Beaumont, Robert Kaczmarczyk, Clayton Mullis, Aarush Katta, Theo Coombes, Jenia Jitsev, and Aran Komatsuzaki. Laion-400m: Open dataset of clip-filtered 400 million image-text pairs. *arXiv preprint arXiv:2111.02114*, 2021. 2
- [65] Piyush Sharma, Nan Ding, Sebastian Goodman, and Radu Soricut. Conceptual captions: A cleaned, hypernymed, image alt-text dataset for automatic image captioning. In *Proceedings of the 56th Annual Meeting of the Association for Computational Linguistics (Volume 1: Long Papers)*, pages 2556–2565, 2018. 2
- [66] Leyang Shen, Gongwei Chen, Rui Shao, Weili Guan, and Liqiang Nie. Mome: Mixture of multimodal experts for generalist multimodal large language models. *arXiv preprint arXiv:2407.12709*, 2024. 2, 3
- [67] Wenhao Shi, Zhiqiang Hu, Yi Bin, Junhua Liu, Yang Yang, See-Kiong Ng, Lidong Bing, and Roy Ka-Wei Lee. Mathllava: Bootstrapping mathematical reasoning for multimodal large language models. *arXiv preprint arXiv:2406.17294*, 2024. 2, 3, 6, 7
- [68] Benny J Tang, Angie Boggust, and Arvind Satyanarayan. Vistext: A benchmark for semantically rich chart captioning. *arXiv preprint arXiv:2307.05356*, 2023. 1
- [69] Gemini Team, Rohan Anil, Sebastian Borgeaud, Yonghui Wu, Jean-Baptiste Alayrac, Jiahui Yu, Radu Soricut, Johan Schalkwyk, Andrew M Dai, Anja Hauth, et al. Gemini: a family of highly capable multimodal models. *arXiv preprint arXiv:2312.11805*, 2023. 7
- [70] Gemini Team, Petko Georgiev, Ving Ian Lei, Ryan Burnell, Libin Bai, Anmol Gulati, Garrett Tanzer, Damien Vincent, Zhufeng Pan, Shibo Wang, et al. Gemini 1.5: Unlocking multimodal understanding across millions of tokens of context. *arXiv preprint arXiv:2403.05530*, 2024. 6
- [71] NovelSeek Team, Bo Zhang, Shiyang Feng, Xiangchao Yan, Jiakang Yuan, Zhiyin Yu, Xiaohan He, Songtao Huang, Shaowei Hou, Zheng Nie, et al. Novelseek: When agent becomes the scientist—building closed-loop system from hypothesis to verification. *arXiv preprint arXiv:2505.16938*, 2025. 3
- [72] Shengbang Tong, Ellis Brown, Penghao Wu, Sanghyun Woo, Manoj Middepogu, Sai Charitha Akula, Jihan Yang, Shusheng Yang, Adithya Iyer, Xichen Pan, et al. Cambrian-1: A fully open, vision-centric exploration of multimodal llms. *arXiv preprint arXiv:2406.16860*, 2024. 1
- [73] Hugo Touvron, Thibaut Lavril, Gautier Izacard, Xavier Martinet, Marie-Anne Lachaux, Timothée Lacroix, Baptiste Rozière, Naman Goyal, Eric Hambro, Faisal Azhar, et al. Llama: Open and efficient foundation language models. *arXiv preprint arXiv:2302.13971*, 2023. 2
- [74] Hugo Touvron, Louis Martin, Kevin Stone, Peter Albert, Amjad Almahairi, Yasmine Babaei, Nikolay Bashlykov, Soumya Batra, Prajjwal Bhargava, Shruti Bhosale, et al. Llama 2: Open foundation and fine-tuned chat models. *arXiv preprint arXiv:2307.09288*, 2023. 2
- [75] Bin Wang, Chao Xu, Xiaomeng Zhao, Linke Ouyang, Fan Wu, Zhiyuan Zhao, Rui Xu, Kaiwen Liu, Yuan Qu, Fukai Shang, et al. Mineru: An open-source solution for precise document content extraction. *arXiv preprint arXiv:2409.18839*, 2024. 2, 3
- [76] Ke Wang, Junting Pan, Weikang Shi, Zimu Lu, Mingjie Zhan, and Hongsheng Li. Measuring multimodal mathematical reasoning with math-vision dataset, 2024. 1
- [77] Peng Wang, Shuai Bai, Sinan Tan, Shijie Wang, Zhihao Fan, Jinze Bai, Keqin Chen, Xuejing Liu, Jialin Wang, Wenbin Ge, et al. Qwen2-vl: Enhancing vision-language model’s perception of the world at any resolution. *arXiv preprint arXiv:2409.12191*, 2024. 2, 5, 6, 8

- [78] Peng Wang, Shuai Bai, Sinan Tan, Shijie Wang, Zhihao Fan, Jinze Bai, Keqin Chen, Xuejing Liu, Jialin Wang, Wenbin Ge, et al. Qwen2-vl: Enhancing vision-language model’s perception of the world at any resolution. *arXiv preprint arXiv:2409.12191*, 2024. 1
- [79] Weiyun Wang, Zhe Chen, Wenhai Wang, Yue Cao, Yangzhou Liu, Zhangwei Gao, Jinguo Zhu, Xizhou Zhu, Lewei Lu, Yu Qiao, and Jifeng Dai. Enhancing the reasoning ability of multimodal large language models via mixed preference optimization. *arXiv preprint arXiv:2411.10442*, 2024. 6
- [80] Haoran Wei, Chenglong Liu, Jinyue Chen, Jia Wang, Lingyu Kong, Yanming Xu, Zheng Ge, Liang Zhao, Jianjian Sun, Yuang Peng, et al. General ocr theory: Towards ocr-2.0 via a unified end-to-end model. *arXiv preprint arXiv:2409.01704*, 2024. 2, 3, 5, 8, 1
- [81] Renqiu Xia, Bo Zhang, Haoyang Peng, Hancheng Ye, Xiangchao Yan, Peng Ye, Botian Shi, Yu Qiao, and Junchi Yan. Structchart: Perception, structuring, reasoning for visual chart understanding. *arXiv preprint arXiv:2309.11268*, 2023. 5, 1
- [82] Renqiu Xia, Mingsheng Li, Hancheng Ye, Wenjie Wu, Hongbin Zhou, Jiakang Yuan, Tianshuo Peng, Xinyu Cai, Xiangchao Yan, Bin Wang, et al. Geox: Geometric problem solving through unified formalized vision-language pre-training. *arXiv preprint arXiv:2412.11863*, 2024. 3, 6
- [83] Renqiu Xia, Song Mao, Xiangchao Yan, Hongbin Zhou, Bo Zhang, Haoyang Peng, Jiahao Pi, Daocheng Fu, Wenjie Wu, Hancheng Ye, et al. Docgenome: An open large-scale scientific document benchmark for training and testing multi-modal large language models. *arXiv preprint arXiv:2406.11633*, 2024. 2, 3, 5, 8, 1
- [84] Renqiu Xia, Bo Zhang, Hancheng Ye, Xiangchao Yan, Qi Liu, Hongbin Zhou, Zijun Chen, Min Dou, Botian Shi, Junchi Yan, et al. Chartx & chartvlm: A versatile benchmark and foundation model for complicated chart reasoning. *arXiv preprint arXiv:2402.12185*, 2024. 1, 2, 3, 5, 8
- [85] Qinghao Ye, Haiyang Xu, Jiabo Ye, Ming Yan, Anwen Hu, Haowei Liu, Qi Qian, Ji Zhang, and Fei Huang. mplug-owl2: Revolutionizing multi-modal large language model with modality collaboration. In *Proceedings of the IEEE/CVF Conference on Computer Vision and Pattern Recognition*, pages 13040–13051, 2024. 1, 2
- [86] Jiakang Yuan, Tianshuo Peng, Yilei Jiang, Yiting Lu, Renrui Zhang, Kaituo Feng, Chaoyou Fu, Tao Chen, Lei Bai, Bo Zhang, et al. Mme-reasoning: A comprehensive benchmark for logical reasoning in mllms. *arXiv preprint arXiv:2505.21327*, 2025. 3
- [87] Xiang Yue, Xingwei Qu, Ge Zhang, Yao Fu, Wenhao Huang, Huan Sun, Yu Su, and Wenhui Chen. Mammoth: Building math generalist models through hybrid instruction tuning. *arXiv preprint arXiv:2309.05653*, 2023. 1
- [88] Dan Zhang, Ziniu Hu, Sining Zhoubian, Zhengxiao Du, Kaiyu Yang, Zihan Wang, Yisong Yue, Yuxiao Dong, and Jie Tang. Sciglm: Training scientific language models with self-reflective instruction annotation and tuning. *arXiv preprint arXiv:2401.07950*, 2024. 1
- [89] Renrui Zhang, Xinyu Wei, Dongzhi Jiang, Yichi Zhang, Ziyu Guo, Chengzhuo Tong, Jiaming Liu, Aojun Zhou, Bin Wei, Shanghang Zhang, et al. Mavis: Mathematical visual instruction tuning. *arXiv preprint arXiv:2407.08739*, 2024. 2, 3, 5, 6, 7, 1
- [90] Renrui Zhang, Dongzhi Jiang, Yichi Zhang, Haokun Lin, Ziyu Guo, Pengshuo Qiu, Aojun Zhou, Pan Lu, Kai-Wei Chang, Yu Qiao, et al. Mathverse: Does your multi-modal llm truly see the diagrams in visual math problems? In *European Conference on Computer Vision*, pages 169–186. Springer, 2025. 2, 3, 5
- [91] Yanzhe Zhang, Ruiyi Zhang, Jiuxiang Gu, Yufan Zhou, Nedim Lipka, Diyi Yang, and Tong Sun. Lllavar: Enhanced visual instruction tuning for text-rich image understanding. *arXiv preprint arXiv:2306.17107*, 2023. 1
- [92] Mingyu Zheng, Xinwei Feng, Qingyi Si, Qiaoqiao She, Zheng Lin, Wenbin Jiang, and Weiping Wang. Multimodal table understanding. *arXiv preprint arXiv:2406.08100*, 2024. 2, 3, 1
- [93] Wenwen Zhuang, Xin Huang, Xiantao Zhang, and Jin Zeng. Math-puma: Progressive upward multimodal alignment to enhance mathematical reasoning. *arXiv preprint arXiv:2408.08640*, 2024. 2, 6, 7
- [94] Zhuofan Zong, Bingqi Ma, Dazhong Shen, Guanglu Song, Hao Shao, Dongzhi Jiang, Hongsheng Li, and Yu Liu. Mova: Adapting mixture of vision experts to multimodal context. *arXiv preprint arXiv:2404.13046*, 2024. 2, 3